https://doi.org/10.5194/egusphere-2023-1676
Preprint. Discussion started: 23 August 2023

Diurnal variation of aerosol indirect effect for warm marine boundary layer clouds in the eastern north Atlantic.

Shaoyue Qiu[1], Xue Zheng[1], David Painemal[2,3], Christopher R. Terai[1], and Xiaoli Zhou[4,5]

[1]Atmospheric, Earth and Energy Division, Lawrence Livermore National Laboratory, Livermore, California, USA
[2] Science Directorate, NASA Langley Research Center, Hampton, VA, USA
[3] Analytical Mechanics Associates, Hampton, VA, USA
[4]Chemical Sciences Laboratory, NOAA, Boulder, CO, USA,
[5]Cooperative Institute for Research in Environmental Sciences (CIRES), University of Colorado, Boulder, CO, USA

Correspondence to: Shaoyue Qiu (qiu4@llnl.gov)

Abstract. Warm boundary layer clouds in the Eastern North Atlantic region exhibit significant diurnal variations in cloud properties. However, the diurnal cycle of the aerosol indirect effect (AIE) for these clouds remains poorly understood. This study takes advantage of recent advancements in the spatial resolution of geostationary satellites to explore the diurnal cycle of AIE by estimating the cloud susceptibilities to changes in cloud droplet number concentration (N_d). Cloud retrievals for four months of July (2018-2021) from SEVIRI on Meteosat-11 over this region are analyzed. Our results reveal a significant "U-shaped" daytime cycle in susceptibilities of cloud liquid water path (LWP), cloud albedo, and cloud fraction. Clouds are found to be more susceptible to N_d perturbations at noon and less susceptible in the morning and evening. The magnitude and sign of cloud susceptibilities depend heavily on the cloud state defined by cloud LWP and precipitation conditions. Non-precipitating thin clouds account for 44% of all warm boundary layer clouds in July and they contribute the most to the observed diurnal variation. Non-precipitating thick clouds are the least frequent cloud state (10%), they exhibit more negative LWP and albedo susceptibilities compared to thin clouds. Precipitating clouds are the dominant cloud state (46%), but their cloud susceptibilities show minimal variation throughout the day.

We find evidence that the diurnal cycle of LWP and albedo susceptibilities for non-precipitating clouds are influenced by a combination of the diurnal transition between non-precipitating thick and thin clouds and the "lagged" cloud responses to N_d perturbations. The diurnal cycle in cloud fraction susceptibility for non-precipitating thick clouds can be attributed to the diurnal variation in cloud morphology (e.g., overcast or broken). The dissipation and development of clouds do not adequately explain the observed variation in cloud susceptibilities. Additionally, diurnal variation of cloud susceptibility is primarily driven by variation in the intensity of cloud response rather than the frequency of occurrence of cloud states. Our results imply that polar-orbiting satellites with overpass time at 13:30 local time underestimate daytime mean value of cloud susceptibility, as they observe susceptibility daily minima in the study region.

https://doi.org/10.5194/egusphere-2023-1676
Preprint. Discussion started: 23 August 2023

1. Introduction

Warm boundary layer clouds, including stratus, stratocumulus, and cumulus clouds, are prevalent over the sub-tropical oceans, account for over 30% of the global annual mean cloud coverage (Warren et al., 1988; Wood, 2012). These clouds have a significant net negative radiative forcing on the surface radiation budget. However, our understanding of the aerosol indirect effect (AIE) on these clouds, particularly the impact of aerosols on cloud amount, brightness, and lifetime, remains a significant source of uncertainty in estimating the radiative forcing from human activities. The AIE plays a critical role in the Earth's radiation budget through its interactions with clouds. It consists of two effects: the Twomey effect, which involves an increase in cloud albedo (α_c) due to smaller droplets (Twomey, 1977), and the cloud adjustment effect, which encompasses the impact of aerosols on cloud amount, cloud water, and α_c through modulating cloud processes (Albrecht, 1989). The Twomey effect has been well-studied and quantified (e.g., Bréon et al., 2003; Feingold et al., 2003; Penner et al.; 2004). The cloud adjustment effect, on the other hand, are highly variable with large uncertainties in signs and magnitudes depending on cloud state, boundary layer, and meteorological conditions among other factors (e.g., Han et al., 2002; Wang et al., 2003; Small et al., 2009; Sato et al, 2018).

Previous studies have made significant progress in identifying different cloud processes and feedback mechanisms to explain the responses of CF, LWP, and α_c to aerosol perturbations (e.g., as summarized in Steven and Feingold, 2009; Fan et al., 2016; Gryspeerdt et al., 2019). The cloud adjustment effect is influenced by two key feedback mechanisms: precipitation suppression, and sedimentation-evaporation-entrainment.

Under clean conditions and for clouds predominantly precipitating, an increase in the cloud droplet number concentration (N_d) decreases droplet sizes, reduces precipitation efficiency and decreases water loss from precipitation. Consequently, this promotes an increase in cloudiness and cloud LWP (Albrecht, 1989; Qian et al., 2009; Li et al., 2011; Terai et al., 2012, 2015). For non-precipitating clouds, decreased cloud drop size due to increases in N_d impacts CF and LWP through their impact on the entrainment rate. A decrease in cloud droplet size diminishes the sedimentation rate in clouds, causing an accumulation of cloud water near the cloud top. This increased cloud water in the entrainment zone enhances cloud-top radiative cooling, entrainment rate, and evaporation, resulting in a decrease in CF and cloud LWP (Bretherton et al., 2007; Chen et al., 2014; Toll et al., 2019; Gryspeerdt et al., 2019).

Additionally, the faster evaporation rates from smaller droplets enhance cloud-top cooling, downward motion in clouds, total kinetic energy, and horizontal buoyancy gradient. The processes listed above, in turn, increase evaporation and entrainment rate and, thus, forming a positive feedback loop (Wang et al., 2003; Xue and Feingold, 2006; Small et al., 2009; Toll et al., 2019). Furthermore, among non-precipitating clouds, thick clouds with larger LWP exhibit stronger cloud-top longwave radiative cooling rate and therefore stronger cloud-top entrainment rate (e.g., Sandu et al., 2008, Williams and Igel, 2021). Therefore, the classification of cloud states (e.g., precipitating conditions and thickness) is essential for accurately quantifying the AIE and discerning opposing cloud processes. In this study, we classify cloud states based on the LWP-N_d parameter space, as these variables provide the most informative metrics for cloud susceptibility (Zhang et al., 2022).

This study focus on the Eastern North Atlantic (ENA) region, where the U.S. Department of Energy (DOE) Atmospheric Radiation Measurement program (ARM) deployed the ground-based user facility at the Azores archipelago (Mather and Voyles, 2013). During the summer over ENA region, warm boundary layer clouds exhibit pronounced diurnal variations in their properties and cloud states. Based on ARM surface radar and lidar observations, the frequency of stratocumulus clouds is highest at night, accompanied by an increase in the fraction of precipitating clouds. Throughout the daytime, both cloud fraction and precipitation fraction experience a slight decrease, followed by an increase after sunset (Remillard et al, 2012). The retrieved cloud microphysical properties from ARM ground-based observations show similar " U-shaped" diurnal variations in cloud LWP, liquid water content, and optical thickness (Dong et al., 2014). Additionally, numerical studies have revealed a distinct diurnal cycle of AIE for marine stratocumulus clouds, attributed to changes in cloud properties, boundary layer thermodynamic conditions, and sea surface temperature (e.g., Sandu et al., 2008, 2009). However, the ARM ground-based observation is at a fixed location without a sufficient spatial coverage, there have been few observational analyses investigating the diurnal cycle of AIE in the ENA region. With recent advancements in the spatial resolution of geostationary satellites, this study aims to investigate the diurnal variation of the AIE in warm boundary layer clouds over the ENA region and gain a better understanding of the underlying mechanisms.

Both cloud properties and meteorological conditions have substantial spatiotemporal variabilities and distinct diurnal variations. Furthermore, changes in meteorological conditions can in turn influence cloud and aerosol properties. One of the main challenges in understanding the AIE lies in isolating the impacts of the confounding meteorological drivers on clouds and aerosols from AIE on clouds. To address this challenge, Gryspeerdt et al. (2016) proposed the use of N_d as an intermediary variable for AIE, instead of using aerosol optical depth (AOD) or aerosol index. The use of N_d circumvents the well-known dependency of AOD on CF and surface wind speed, which does not necessarily reflect actual changes in aerosol loading. Moreover, the control of relative humidity and aerosol type on AOD prevents to establish a direct link between AOD and aerosol concentration or cloud condensation nuclei (CCN).

Another common method to disentangle meteorological impacts is to sort the controlling meteorological factors of cloud state, such as relative humidity, lower tropospheric stability, vertical velocity, and examine the AIE accordingly (e.g., Chen et al., 2014; Gryspeerdt et al., 2019). However, this approach overlooks important information, including the frequency of occurrence of specific environmental conditions, the spatiotemporal co-variation of meteorological factors, and the correlations among them. Zhou et al. (2021) and Zhang et al. (2022) proposed a new aspect to estimate the cloud susceptibility within a $1° \times 1°$ grid box of each satellite snapshot by assuming consistent meteorological conditions within this spatial domain. Additionally, it is important to note that meteorological conditions influence albedo susceptibility by altering the frequency of occurrence of different cloud states (e.g., precipitating and non-precipitating). Specifically, within a particular cloud state, meteorological conditions offer limited information regarding cloud susceptibility (Zhang et al, 2022).

The second main source of uncertainty in observational AIE studies arise from inferring processes in a temporally evolving system based on snapshots of observations (Mülmenstädt and Feingold, 2018). Due to the limited temporal or spatial resolution of the observations, most studies assume a Markovian system, where clouds and AIE are assumed to only relate to the current state of the system and have no memory of the past states. However, this assumption contradicts the nature of the cloud system. Recent advancements in the spatiotemporal resolutions of the geostationary satellite offer an opportunity to address this issue. For instance, Christensen et al. (2020) tracked the influence of aerosols on cloud lifetime and development at different cloud stages, and Gryspeerdt et al. (2021) quantified the timescale of aerosols' impact on CF and LWP. Nonetheless, the direct evaluation of the impact of cloud memory on quantified cloud susceptibility remains unexplored.

To facilitate a process-level understanding of the drivers behind the diurnal variation, we will classify warm boundary layer clouds into three states: precipitating clouds, non-precipitating thick clouds, and non-precipitating thin clouds. We investigate the changes in both the frequency of occurrence and the intensity of AIE for different cloud states throughout the day. Additionally, we track the temporal changes in cloud state within each fixed $1° \times 1°$ grid box and quantify the influences of cloud memory and state transition on AIE. Section 2 describes the datasets as well as the methodology employed to quantify cloud susceptibilities, distinguish precipitating clouds from the satellite retrievals, and track cloud states. We present our results in Section 3. Section 3.1 characterizes the general conditions of warm boundary clouds over the ENA region during the summer. Section 3.2 introduces the LWP-N_d parameter space and illustrates the dependence of cloud responses to N_d perturbations on cloud states. We then, discuss the mean diurnal variation of cloud susceptibilities for all cloud states in Section 3.3, followed by

https://doi.org/10.5194/egusphere-2023-1676
Preprint. Discussion started: 23 August 2023

an analysis on the diurnal variation of AIE for each cloud state and the impact of the state transition on AIE in Section 3.4. In Section 3.5, we decompose the contributions to the diurnal variation of cloud susceptibility into two components, one is from changes in the frequency of occurrence of different cloud states and the other is from changes in the intensity of AIE during the day. Section 4 includes discussions on the similarities and differences in findings between this study and previous studies of AIE and Section 5 is the summary and conclusions of this study.

2. Dataset and Methodology

We use cloud retrievals derived from the Spinning Enhanced Visible InfraRed Imager (SEVIRI) on Meteosat-11, with a spatial resolution of 3 km at nadir and a half-hourly temporal resolution over the ENA region (33-43°N, 23-33°W). SEVIRI cloud products are derived using the Satellite ClOud and Radiation Property retrieval System (SatCORPS) algorithms (e.g., Painemal et al., 2021), based on the methods applied by the Clouds and the Earth's Radiant Energy System (CERES) project, and specifically tailored to support the ARM program over the ARM ground-based observation sites (Minnis et al. 2011, 2020). Given the purpose of this study on quantifying the AIE on warm boundary layer clouds, we focus on four months of July (2018-2021), a period that coincides with the highest frequency of occurrence of warm boundary layer clouds over the ARM ENA site (Rémillard et al. 2012; Dong et al., 2014, 2023).

The cloud mask algorithm implemented in SatCORPS is described in Trepte et al. (2019). SatCORPS cloud properties are based on the shortwave-infrared split-window technique during daytime (VISST, Minnis et al. 2011, 2020), with cloud optical depth (τ) and effective radius (r_e) being derived using an iterative process that combines reflectance and brightness temperatures from the 0.64 µm and 3.9 µm channels. Cloud LWP is computed from τ and r_e using the formula $LWP = \frac{4 r_e \tau}{3 Q_{ext}}$, where Q_{ext} represents the extinction efficiency and assumed constant of 2.0. The top-of- atmosphere (TOA) broadband shortwave α_c is derived from an empirical radiance-to-broadband conversion using the satellite imager's visible channel and CERES Single Scanning Footprint (SSF) shortwave fluxes, and dependent on solar zenith angle and surface type (Minnis et al. 2016). Cloud top height computations follow the methodology in Sun-Mack et al. (2014).

To validate the Meteosat-11 retrieved cloud mask and the detection of boundary layer clouds, we compare the boundary layer cloud fractions derived from Meteosat-11 with the ground-based observations at the ARM ENA site. As seen in Figure S1, both the diurnal variation and the mean CF of Meteosat-11 agree well with ARM observations. More details on the methodology for the evaluation study are included in the supplementary material.

Our analysis focuses on warm boundary layer clouds with cloud tops below 3km and a liquid cloud phase. To focus specifically on boundary layer cloud cases without including the edges of deep clouds, we apply a stricter threshold than merely using the pixel-level cloud top height. We define boundary layer clouds as those with 90% of their cloud tops below 3km, labeling all contiguous cloudy pixels as distinct cloud objects.

Cloud N_d is retrieved based on the adiabatic assumptions for warm boundary layer clouds, as in Grosvenor et al. (2018) according to the following equation:

$$N_d = \frac{\sqrt{5}}{2\pi k} \left(\frac{f_{ad} c_w \tau}{Q_{ext} \rho_w r_e^5}\right)^{1/2} \quad (1)$$

In Equation (1), k represents the ratio between the volume mean radius and r_e, assumed to be constant of 0.8 for stratocumulus; f_{ad} is the adiabatic fraction of the observed liquid water path and assumed to be 0.8 for stratocumulus clouds (Brenguier et al., 2011; Zuidema et al., 2012); c_w is the condensation rate, which is a function of cloud temperature; Q_{ext} is the extinction coefficient, approximated as 2 in this study; and ρ_w is the density of liquid water. While the different components of Eq. (1) could contribute to the uncertainties in N_d, errors in r_e are the dominant drivers in Eq. (1) (Grosvenor et al., 2018).

To minimize uncertainties associated with bias in satellite cloud microphysical retrievals, we only select pixels with a minimum r_e of $3\mu m$, a minimum τ of 3, and a solar zenith angle (SZA) of less than 65° (e.g., Painemal et al., 2013; Painemal, 2018; Zhang et al., 2022). The SZA threshold of 65° was chosen to minimize biases observed at high solar zenith angle in r_e and τ (e.g. Grosvenor & Wood, 2014; Grosvenor et al., 2018).

In addition, to reduce the uncertainties associated with the adiabatic assumption in the N_d retrieval, we implement a filtering process. For each cloud, we exclude cloud pixels at the cloud edge, defined as those adjacent to a cloud-free pixel, following a similar sampling strategy suggested by Gryspeerdt et al. (2022). Therefore, all cloud properties in this study refer to the properties of cloud body without cloud edge. It is worthy of note that shallow cumulus clouds with diameters smaller than 9km are not included. The removal of cloud edge pixels accounts for ~14% of the cloudy pixels. Furthermore, we removed grid boxes containing islands due to the uncertainties in Meteosat retrievals over contrasting underlying surface (not shown). Lastly, to avoid unrealistically large retrievals, we eliminate pixels with the retrieved N_d values exceeding 1000 cm^{-3}, which constituted only 0.002% of the data.

Cloud susceptibility is quantified as the slopes between cloud properties and N_d using a least-square regression. To facilitate the analysis, we first average the 3-km cloud retrievals to a regular 0.25° × 0.25° grid for each half-hourly time step. This grid averaging process helps to eliminate spatial correlations arising from small-scale cloud processes and reduces the influence of extreme values on the regression slopes. To further mitigate the impact from spatial and temporal covariability of cloud properties and N_d on the derived relationships, cloud susceptibility is estimated within a 1° × 1° grid box at each satellite time step (e.g., Zhou et al., 2021; Zhang et al, 2022). Estimating the cloud susceptibility over a confined space also help to constrain the meteorological impacts on AIE, with the assumption of a homogeneous meteorological condition within this spatial scale. Next, susceptibilities are calculated using the 0.25° smoothed data if the number of data points within the 1° × 1° box exceeds six (a maximum of 16 data points). It is important to note that when computing the mean cloud properties at the 0.25° resolution, only data from cloudy pixels are used to ensure that the estimated susceptibility is not weighted by CF. Lastly, due to the minimal spatial variability of cloud susceptibility in the study region, the 1° cloud susceptibility is averaged over the study region to characterize the diurnal variation of AIE. Additionally, results and conclusions of this study are not sensitive to the size of the box calculating the cloud susceptibility (e.g., over a 0.8° × 0.8° box or over a 1.5° × 1.5° box, not shown).

Because of the nonlinear relationships between LWP and N_d, the LWP susceptibility is defined as the slope of the log-log regressions $dln(LWP)/dln(N_d)$ (e.g., Gryspeerdt et al. 2019). The albedo susceptibility is estimated as the slope of change in α_c with N_d perturbations as $d\alpha_c/dln(N_d)$ (e.g., Painemal 2018). The CF susceptibility is estimated as $dCF/dln(N_d)$. The mean CF is defined as the fraction of cloudy pixels excluding cloud edge to the sum of cloudy and clear pixels within each 0.25° × 0.25° box, and cloudy pixels at cloud edge are set as clear. Removing the cloud edge decreases the four-month mean CF for warm boundary layer clouds from 21.6% to 19.0%.

The susceptibility of the shortwave radiative fluxes to N_d (F_0) is estimated as the sensitivity of the TOA shortwave upward radiative flux (SW_{TOA}^{up}) to N_d perturbations (e.g., Chen et al. 2014; Painemal 2018; Zhang et al. 2022). The mean SW_{TOA}^{up} over a 1° × 1° grid box is estimated using Eq. (2), with the assumption that the clear-sky albedo over the ocean is small compared to the cloud albedo:

$$\overline{SW_{TOA}^{up}} = \overline{SW_{TOA}^{dn}} \cdot \overline{\alpha_c} \cdot \overline{CF}, \qquad (2)$$

https://doi.org/10.5194/egusphere-2023-1676
Preprint. Discussion started: 23 August 2023

where SW_{TOA}^{dn} is the grid-box mean TOA shortwave downward radiative flux, which is estimated based on the latitude, longitude, date, and overpass time of each pixel, α_c and CF are the grid-box mean values. Then, F_0 is estimated using the calculated α_c and CF susceptibilities, and the 1° × 1° grid-box mean cloud properties as shown in the equation below:

$$F_0 = -\frac{dSW_{TOA}^{up}}{dln(N_d)} = -\overline{SW_{TOA}^{dn}} \cdot \left(\frac{d\alpha_c}{dln(N_d)} \cdot \overline{CF} + \frac{dCF}{dln(N_d)} \cdot \overline{\alpha_c}\right). \quad (3)$$

F_0 is in the unit of $W\ m^{-2}\ ln\ (N_d)^{-1}$, and a positive value indicates a decrease in the SW_{TOA}^{up}, which is a *warming* effect to the surface.

To minimize uncertainties in the linear regression for the estimated susceptibility, we analyze regressions that exhibited a goodness of fit exceeding the 95% confidence interval (i.e., $\chi^2 < \chi^2_{0.95,c}$), and an absolute correlation coefficient greater than 0.2 (e.g., Painemal, 2018; Zhang et al., 2022). There is a total of ~95,000 samples of the 1° cloud susceptibilities in this study, applying the goodness of fit thresholds result in an exclusion of ~ 22,000 samples, which is ~23% of the data. Sensitivity test shows that including cases that fail the goodness of fit test will not change the results and conclusions of this study (not shown). More specifically, including these cases decrease the magnitude of cloud susceptibilities for all three cloud states, but the signs of cloud responses to N_d perturbations remain consistent.

Since precipitating and non-precipitating clouds exhibit distinct responses to aerosol perturbations due to the effect of precipitation suppression and the wet-scavenging feedback, it is critical to distinguish between these two cloud states when estimating AIE. Previous studies have utilized various methods based on the effective radius threshold (e.g., Gryspeerdt et al., 2019, Toll et al., 2019; Zhang et al., 2022) and the rain rate threshold (e.g., Duong et al., 2011; Terai et al., 2015) from satellite retrievals. In our study, we validate these two methods using the precipitating mask estimated from ground-based observations with a radar reflectivity threshold together with the lidar-defined cloud base at the ARM ENA site (e.g., Wu et al., 2020). The thresholds of r_e >12 μm and r_e >15 μm yield hit rates of 0.79 and 0.73, respectively. However, the false alarm rate is higher for r_e >12 μm (0.21) compared to r_e >15 μm (0.1). Rain rate is computed using the empirical relationships derived from ground-based measurements in Comstock et al. (2004) as $R = 0.0156\ ({}^{LWP}/_{N_d})^{1.75}$. Using a threshold of R>0.05 mm/h results in a hit rate of 0.65. Consequently, we use the r_e >15 μm threshold to define precipitating clouds.

To investigate the dependences of AIE on previous cloud states and quantify the influence of cloud memory on the estimated cloud susceptibility, we opt for tracking the historical cloud state over a fixed location with time, rather than tracking cloud parcels in space and time. A two-hour tracking window is used to define changes in cloud state over the 1° × 1° grid box. Given the typical boundary layer mean wind speed, horizontal advection would have limited impact on cloud state transition. Section 3.4 includes more details and discussions on the sensitivity of tracking time and the influence of advection on our classification. The influence of cloud memory is assessed by comparing the cloud susceptibilities of clouds that undergo a transition in cloud state with those that do not experience such a transition.

3. Results

3.1 General cloud conditions and mean cloud responses to N_d perturbations

In the ENA region, characterized by dominant Bermuda High with its prevailing ridge and zonal synoptic pattern (Mechem et al., 2018), the summer season gives rise to the annual peak in boundary layer cloud coverage at ENA. The monthly mean low-level CF retrieved from Meteosat-11 reaches its maximum of 35% in July, compared to an annual mean of 17% during the four-year study period (not shown).

https://doi.org/10.5194/egusphere-2023-1676
Preprint. Discussion started: 23 August 2023

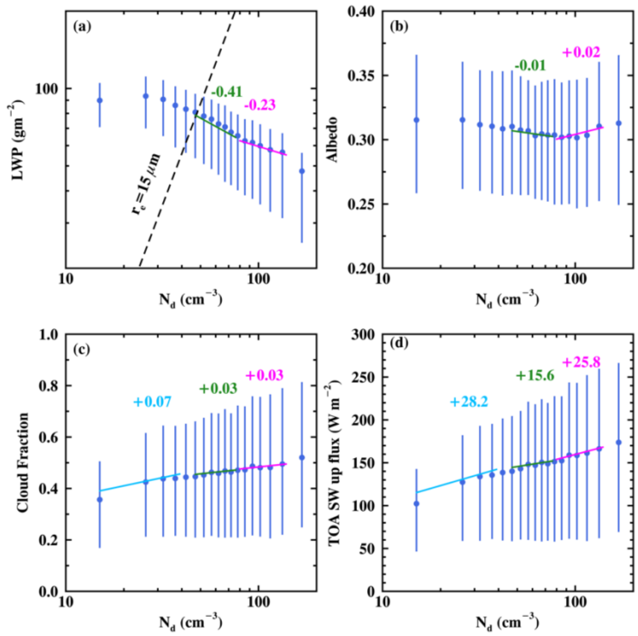

Figure 1. Relationships between N_d and cloud properties: (a) cloud LWP, (b) cloud albedo, (c) cloud fraction, and (d) TOA shortwave upward radiative flux. The dots represent the mean values, while the whiskers indicate the upper and lower 25th percentile. In (a), the dashed line denotes r_e =15 μm, serving as an indicator of precipitation occurrence, with precipitating clouds located to the left of the line. Blue, green, and magenta lines in panels (a)-(d) represent the regression slopes of the mean cloud properties, and the mean $ln(N_d)$, for N_d < 40 cm^{-3}, N_d between 40 and 80 cm^{-3}, and N_d > 80 cm^{-3}, respectively.

This region represents a typical clean marine condition, situated far from continental influences, which results in a consistently lower N_d compared to polluted marine regions, such as the northeastern (NE) Pacific near California or the northwestern Atlantic near the Gulf of Maine. In July, the mean N_d over the ENA region is 65 cm^{-3} with the lower 5th and upper 95th percentile of 15 and 160 cm^{-3}, respectively. The retrieved N_d values closely align with in-situ measurements from the Aerosol and Cloud Experiments in Eastern North Atlantic (ACE-ENA) field campaign. For instance, the in-situ measured N_d in July 2017 varied from 25 to 150 cm^{-3}, with a mean value of 65 cm^{-3} (e.g., Yeom et al., 2021; Zhang et al., 2021). Moreover, our satellite N_d exhibits good agreement with retrievals based on ground-based observations at the ARM ENA site (e.g., Dong et al., 2014; Wu et al., 2020) and the MOderate resolution Imaging Spectroradiometer (MODIS, e.g., Bennartz 2007; Bennartz and Rausch 2017).

Previous studies have demonstrated that clouds exhibit diverse responses to aerosol perturbations under clean and polluted conditions (e.g., Fan et al. 2016; Mülmenstädt and Feingold, 2018). Cloud properties derived from satellite retrievals show consistent distinct responses under clean (low N_d) and polluted (high N_d) conditions. Figure 1 shows the relationships between the climate mean cloud properties, derived from the pixel-level SEVIRI cloud products, and averaged to the 1° × 1° resolution, as a function of the 1° × 1° mean N_d values. To quantify these responses, cloud susceptibility is estimated as the slope the mean cloud variable changes across N_d bins.

In pristine conditions (N_d < 40 cm^{-3}, ~28% of data), clouds predominantly precipitate (r_e >15 μm, Fig. 1a). The mean cloud LWP features a slight increase followed by a decrease with increasing N_d. This result departs from the precipitation suppression hypothesis, in which LWP typically increases. The absence of a precipitation suppression signal is likely attributed to the relatively modest precipitation witnessed by clouds in this region during summer (e.g., Wu et al., 2020; Zheng and Miller, 2022), where the effect of precipitation suppression is minimal and the entrainment drying effect dominates. In terms of α_c, the

https://doi.org/10.5194/egusphere-2023-1676
Preprint. Discussion started: 23 August 2023

potential decrease in α_c resulting from the decreased LWP offsets the potential increases in α_c caused by the Twomey effect, resulting in a net zero change in mean α_c for clouds with N_d < 40 cm^{-3} (Fig. 1b). Furthermore, the majority of precipitating clouds are broken clouds, with the mean CF that increases with N_d from 0.35 to 0.45 (Fig. 1c). Consequently, the mean SW_{TOA}^{up} flux increases from 100 to 140 $W\ m^{-2}$ as N_d increases from 10 to 40 cm^{-3}. This increase in CF for precipitating clouds aligns with previous study over the north Atlantic region across all seasons (e.g., Gryspeerdt et al., 2016). In summary, despite the slight decrease in mean LWP with increasing N_d for precipitating clouds, the mean cloud albedo remains relatively constant, while the mean CF increases, resulting in an overall increase in the TOA reflected shortwave flux by clouds.

Under relatively polluted conditions with N_d > 40 cm^{-3} (~72% of data), the mean LWP shows a decreasing trend withN_d. For N_d values between 40-80 cm^{-3}, the ln(LWP)- $ln(N_d)$ slope is -0.41, while for N_d exceeding 80 cm^{-3}, the slope reaches -0.23 (green and magenta lines in Fig. 1a). This negative adjustment of LWP for non-precipitating clouds is consistent with the sedimentation-evaporation-entrainment hypothesis, as well as with previous studies of stratocumulus clouds in other regions (e.g., Gryspeerdt et al., 2019; Zhang et al., 2022). The mean α_c remains nearly constant within the N_d range of 40-80 cm^{-3} (Fig. 1b). As LWP decreases at a slower rate for N_d >80 cm^{-3}, the Twomey effect becomes more dominant and leads to a slight increase in α_c with a slope of 0.02 (magenta line in Fig. 1b). For non-precipitating clouds, the mean CF slightly increases with increasing N_d with a CF susceptibility of 0.03 (green and magenta lines in Fig. 1c). As a result, the SW_{TOA}^{up} flux exhibit a weaker susceptibility compared to precipitating clouds (Fig. 1d).

3.2 Daytime mean cloud susceptibilities in the LWP-N_d space

One limitation of the relationships derived from the mean cloud properties with sorted N_d is the confounding effect from meteorological impacts on cloud properties and cloud susceptibilities. As a comparison, Fig. 2 shows the mean cloud susceptibility estimated within each half-hourly snapshot’ s 1° × 1° grid box and averaged in the LWP-N_d parameter space. There are ~ 73,000 samples of the 1° cloud susceptibilities in this study. We calculate the mean susceptibilities for LWP-N_d bins with more than 100 cloud susceptibility samples.

With the assumption that the meteorological condition is homogeneous in each grid box, the estimated cloud susceptibilities exhibit much stronger relationships for all cloud variables compared to the climatological mean adjustment rates shown in Fig. 1. The disparities between the two methods suggest that meteorological influences on clouds likely dampen the signal of the AIE over the ENA region. Moreover, the cloud responses from both for precipitating and non-precipitating clouds exhibit consistent signs between the half-hourly (Fig. 2) and climatological-mean approaches (Fig. 1). This consistency is likely attributed to the confined domain (a 10° × 10°) and the focus on July in this study, which limit the spatial and temporal covariability between cloud properties and N_d. This consistency also demonstrates that the overall cloud responses to N_d perturbations primarily depend on cloud states (e.g., precipitating conditions and cloud thickness).

The dependence of cloud response on cloud state is illustrated in Fig. 2. We define three cloud states*:* (1) *the precipitating clouds (r_e>15 μm),(2) the non-precipitating thick clouds (r_e<15 μm, LWP > 75 gm^{-2}),* and (3) *the non-precipitating thin clouds (r_e<15 μm, LWP < 75 gm^{-2}),* similar to the definition in Zhang et al. (2022).

https://doi.org/10.5194/egusphere-2023-1676
Preprint. Discussion started: 23 August 2023

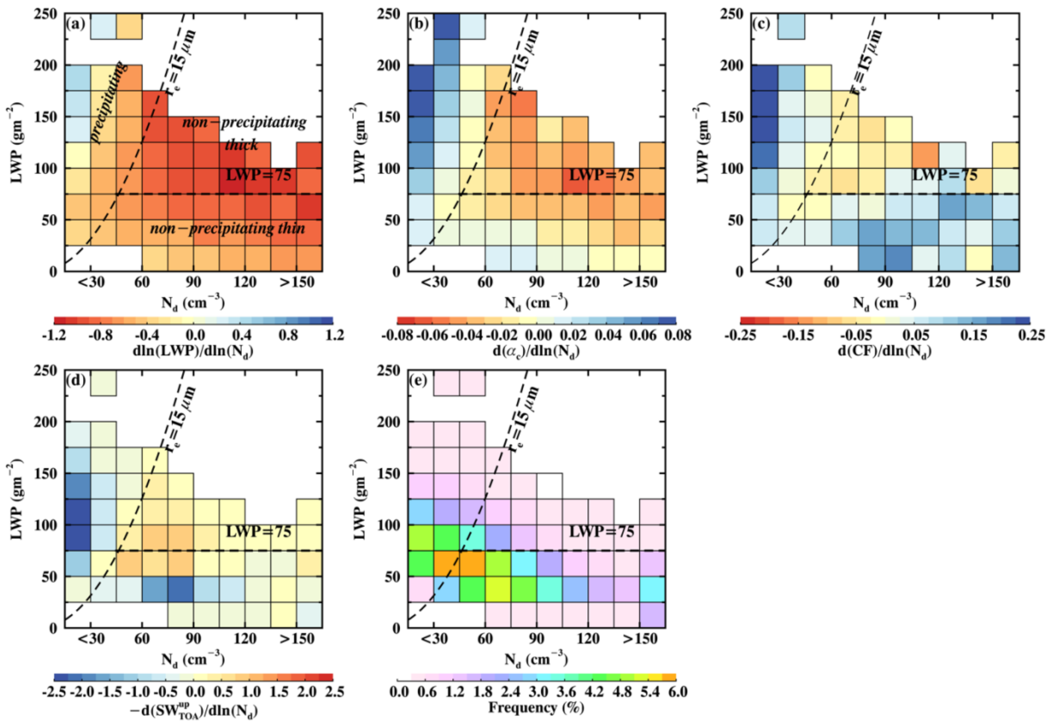

Figure 2. Mean cloud susceptibilities for different N_d and LWP bins during the daytime. (a) cloud LWP susceptibility ($dln(LWP)/dln(N_d)$), (b) cloud albedo susceptibility ($d\alpha_c/dln(N_d)$), (c) cloud fraction susceptibility ($dCF/dln(N_d)$), (d) cloud shortwave susceptibility ($-dSW_{TOA}^{up}/dln(N_d)$) weighted by the frequency of occurrence of samples of each bin, and (e) frequency of occurrence of samples in each bin. The dashed lines in (a)-(e) indicate r_e =15 μm and LWP= 75 gm^{-2}, as thresholds for precipitation (precipitating clouds located to the left of the line) and thick clouds (with LWP > 75 gm^{-2}). The defined three clouds states are noted in (a).

a. Precipitating clouds

Among warm boundary layer clouds, precipitating clouds are the dominant cloud state in July over the study region, the total frequency of occurrence is 46% (Fig.2e). The increase in cloud LWP with N_d is observed primarily in heavily precipitating thick clouds with N_d < 30 cm^{-3} and LWP > 125 gm^{-2} (Fig. 2a). However, these clouds occur relatively infrequently at ENA, accounting for only 2% of the total warm boundary cloud population (Fig. 2e). In contrast, most of the precipitating clouds at ENA are lightly precipitating with 15 < r_e <20 μm (Fig.2e and Fig. S2c) and they exhibit a slight decrease of LWP with N_d (Fig. 2a). LWP susceptibility for lightly precipitating clouds ranges from −0.5 to −0.2, with a mean value of −0.4. The slight decrease in LWP for lightly precipitating clouds aligns with previous findings over the Pacific, Atlantic, and global oceans for marine stratocumulus (e.g., Fig S4 in Zhang and Feingold, 2023).

The contrasting response of LWP to N_d perturbations for lightly and heavily precipitating clouds can be attributed to the interplay of two competing processes: the depletion caused by the sedimentation-evaporation-entrainment feedback and the accumulation resulting from the precipitation suppression feedback. Heavily precipitating clouds are predominantly overcast with a mean CF of 0.65 (Fig. S2a) and a mean r_e of 25 μm (Fig. S2c). Precipitation acts to stabilize the boundary layer, remove water from cloud top, and reduce the entrainment rate (Sandu et al., 2007, 2008). Precipitation suppression and entrainment weakening work in concert and result in a net increase in LWP with increasing N_d. In lightly precipitating clouds, however, the

https://doi.org/10.5194/egusphere-2023-1676
Preprint. Discussion started: 23 August 2023

suppression effect of drizzle on the entrainment rate is minimal. Therefore, the decrease in LWP from entrainment overpowers the increases in LWP from precipitating suppression, leading to a net decrease in LWP with increasing N_d.

Precipitating clouds generally exhibit brighter cloud albedo with increasing N_d as a result of the weak negative and positive LWP adjustment, particularly in heavily precipitating clouds. The α_c susceptibilities range from 0.02 to 0.07 $ln(N_d)^{-1}$. The suppression of precipitation by N_d also lead to a significant increase in CF for heavily precipitating clouds, with slopes greater than 0.25 $ln(N_d)^{-1}$ (Fig. 2c). The CF susceptibilities for lightly precipitating clouds show variation between $\pm$0.025 $ln(N_d)^{-1}$. Considering the combined effects of increased α_c and CF, the total radiative response for precipitating clouds amounts to $-13\ W\ m^{-2} ln(N_d)^{-1}$, which is a summation of the shortwave susceptibility in Figure 2d for bins classified as precipitating clouds. The contributions from CF and α_c effects of -9.5 and $-3.5\ W\ m^{-2}\ ln(N_d)^{-1}$, respectively (Eq. 3).

b. Non-precipitating thick clouds

Non-precipitating thick clouds are less frequent, the total frequency of occurrence is 10% (Fig. 2e). For non-precipitating clouds, the responses of cloud LWP to N_d perturbations differ from that of precipitating clouds. The intensified evaporation from small droplets at high N_d concentrations (e.g., Xue and Feingold, 2006; Small et al., 2009) and the enhanced entrainment due to large LWP (e.g., Sandu et al., 2008, Williams and Igel, 2021) lead to a minimum in LWP susceptibilities of -1.2 at the high-LWP and high-N_d ends (Fig. 2a). As LWP and N_d decrease, the LWP susceptibility gradually increases from -1.2 to -0.5. The mean LWP susceptibility for non-precipitating thick clouds is -0.94. Consistent with the negative LWP susceptibility, non-precipitating thick clouds become less reflective with N_d for all N_d bins with LWP > 75 gm^{-2} (Fig. 2b). Due to the enhanced entrainment and evaporation with increasing N_d, the CF also decreases for non-precipitating thick clouds with CF susceptibilities ranging from -0.05 to -0.1 $ln(N_d)^{-1}$ (Fig. 2c). Considering the decrease in both α_c and CF, non-precipitating thick clouds exhibit a warming effect on the surface, the total radiative response is $+4.4\ W\ m^{-2}\ ln(N_d)^{-1}$ (Fig. 2d).

c. Non-precipitating thin clouds

Non-precipitating thin clouds are more common than thick clouds during summer, with a total frequency of occurrence of 44% (Fig. 2e). Compared to non-precipitating thick clouds, they exhibit less negative LWP and α_c susceptibilities, but with an opposite increasing trend in CF (Figs. 2b, c). The opposite signs in LWP and CF susceptibilities for non-precipitating thin clouds cannot be solely explained by the evaporation-entrainment feedback. In the next section, two additional hypotheses regarding the development/dissipation of clouds and the transition of cloud states will be tested (Table 1). Due to increases in CF, non-precipitating thin clouds have a cooling effect on the surface, with the radiative response of $-4.3\ W\ m^{-2}\ ln(N_d)^{-1}$ (Fig. 2d).

To sum up, the responses of cloud LWP, α_c, and CF to N_d perturbations depend on the cloud states. Precipitating clouds mostly become thinner and brighter with increasing N_d, accompanied by an increase in CF. An increase in LWP with increasing N_d is observed only for heavily precipitating clouds with N_d < 30 cm^{-3} and LWP > 125 gm^{-2}. Non-precipitating thick clouds become thinner, less reflective from TOA, and decrease in cloudiness with N_d perturbations. On the other hand, non-precipitating thin clouds become slightly thinner and less reflective, but their cloudiness increase as N_d increases. Given the dependence of AIE on cloud state, the cloud state classification established here will be applied in the next two sections to facilitate a process-level understanding of cloud responses and the diurnal variation in cloud susceptibilities.

3.3 Diurnal variation of cloud susceptibility

As discussed in the introduction, warm boundary layer clouds exhibit a distinct diurnal cycle in both cloud properties and frequency of occurrence of cloud states during summer. In this section, we investigate the diurnal variation of cloud

https://doi.org/10.5194/egusphere-2023-1676
Preprint. Discussion started: 23 August 2023

susceptibility from 9 to 18 local standard time (LST) using the half-hourly Meteosat-11 retrievals. The mean diurnal variation of satellite-based cloud susceptibility is estimated from each half-hourly time step within each 1° × 1° box and then averaged over the study domain (33-43°N, 23-33°W) during the four months. Over the study domain, there is little spatial variability in cloud susceptibilities and the diurnal cycle of the cloud susceptibility over the 1° × 1° box at the ARM ENA site agree well with the domain mean pattern (not shown). Furthermore, diurnal cycle of the cloud microphysical properties (e.g., r_e, τ, LWP, N_d) show little difference between the domain mean value or that averaged over the 1° × 1° box at the ARM ENA site. The cloud microphysics retrievals from Meteosat-11 agree well with retrievals based on ground-based radar and lidar observations in the diurnal variation (not shown). Therefore, the ARM ENA site at the Azores archipelago can represent the cloud properties and the AIE for warm boundary layer clouds over the study region.

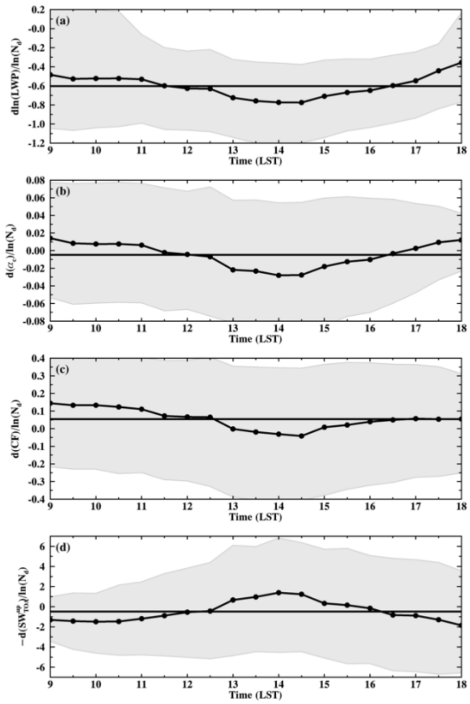

Figure 3. Daytime variation of cloud susceptibilities. (a) cloud LWP susceptibility ($dln(LWP)/dln(N_d)$), (b) cloud albedo susceptibility ($d\alpha_c/dln(N_d)$), (c) cloud fraction susceptibility ($dCF/dln(N_d)$), and (d) cloud shortwave susceptibility ($-dSW_{TOA}^{up}/dln(N_d)$). The shaded areas represent the lower and upper 25th percentile of the cloud susceptibilities for each time step. The black solid lines without symbols in (a)-(d) represent the daytime mean values of cloud susceptibilities.

Warm boundary layer clouds reveal distinct and significant diurnal variations in cloud susceptibilities (Fig. 3). For example, the mean LWP susceptibility exhibits a magnitude of change of 0.4 from morning to noon, which corresponds to approximately 30-40% of the overall variability in LWP susceptibility (Fig. 3a). Similarly, the α_c and CF susceptibility undergo magnitude of diurnal changes of approximately 20-30% compared to the overall variability (Figs. 3b and c). The high variability in cloud susceptibility highlights the complex interplay between synoptic conditions that varies diurnally and cloud states in the ENA region. The diurnal variation of cloud susceptibility is statistically significant at a 95% confidence level based on a student's t-test. Interestingly, all three cloud variables exhibit a "U-shaped" diurnal cycle in cloud susceptibilities with less negative/more positive values in the morning and evening and more negative valuers at noon. Additionally, the α_c and CF susceptibilities switch signs from positive in the morning to negative at noon, and then become positive again in the evening. As

https://doi.org/10.5194/egusphere-2023-1676
Preprint. Discussion started: 23 August 2023

both α_c and CF increase with increasing N_d in the morning, AIE has a cooling effect on the surface and the estimated shortwave susceptibility is $-1.4\ W\ m^{-2}\ ln(N_d)^{-1}$. During 13-16 LST, the shortwave susceptibility switches sign to a warming effect of $+1.2\ W\ m^{-2}\ ln(N_d)^{-1}$ (Fig. 3d).

Given the pronounced diurnal variation of cloud susceptibility, *how can we explain this distinct diurnal variation, and which state of cloud contributes most to the diurnal variation?* One possible explanation is the increased occurrence of precipitating clouds in the morning and evening during summer (Remillard et al, 2012), which increase cloud susceptibility, as depicted in Fig. 2. To investigate this hypothesis and quantify the impacts of different cloud states on the variabilities of cloud susceptibilities, we examined the diurnal variation of cloud susceptibility for each cloud state, along with the diurnal shift in cloud state occurrence frequency.

3.4 Diurnal variation of cloud susceptibility for different cloud states

3.4.1 Non-precipitating thin clouds

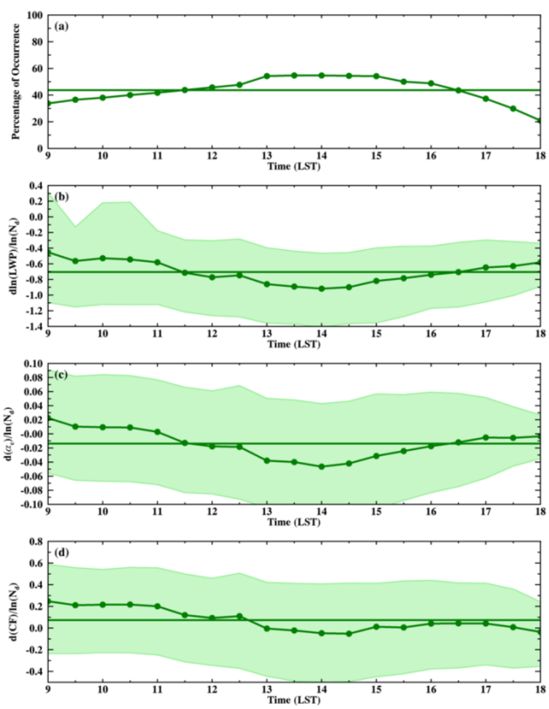

Figure 4. Daytime variation of (a) percentage of occurrence of non-precipitating thin clouds to warm boundary layer clouds, (b) cloud LWP susceptibility ($dln(LWP)/dln(N_d)$), (c) cloud albedo susceptibility ($d\alpha_c/dln(N_d)$), and (d) cloud fraction susceptibility ($dCF/dln(N_d)$) for non-precipitating thin clouds. The shaded areas represent the lower and upper 25th percentile of the cloud susceptibilities for each time step. The solid lines without symbols in (a)-(d) represent the daytime mean values.

Non-precipitating clouds mainly consist of thin clouds, with a daytime mean occurrence of 44% (Fig. 4a). The highest occurrence of non-precipitating thin clouds is observed around noon, consistent with ground-based radar reflectivity measurement at the ENA site (Remillard et al, 2012). Furthermore, as seen in Fig. 4, not only the frequency of cloud occurrence, but also the susceptibilities of LWP, α_c, and CF show distinct diurnal fluctuations. For example, the LWP susceptibility decreases from -0.4 to -0.9, and the α_c susceptibility decreases from 0.02 to $-0.04\ ln(N_d)^{-1}$ from morning to noon, followed by increases in both LWP and α_c susceptibilities in the afternoon. The CF susceptibility is highly positive in the morning and

https://doi.org/10.5194/egusphere-2023-1676
Preprint. Discussion started: 23 August 2023

decreases to near zero after 13 LST. In addition, cloud susceptibility for thin clouds in the morning is statistically significantly different than that at noon and in the evening at a 95% confidence level.

To explain the decrease of cloud susceptibility of non-precipitating thin clouds from morning to noon, we test two hypotheses (H2 and H3 in Table 1). Hypothesis H3 is related to the dissipation of thin clouds during this time period, which is caused by increased solar radiation and decreased LWP. During the dissipation, if homogeneous mixing dominates, both LWP and r_e decrease. As r_e is raised to the power of $-\frac{5}{2}$ in Eq. (1) compared to τ being raised only to the power of $\frac{1}{2}$, the decreases of LWP and r_e could result in an increase in the retrieved N_d. The decreased LWP and increased N_d leads to a decrease in LWP susceptibility (Gryspeerdt et al., 2019). To examine this hypothesis, non-precipitating thin clouds are classified as: growing, dissipating, or constant based on the changes in the mean CF, cloud susceptibilities for the three groups are shown in Figure S4. More specifically, we calculate the change in the mean CF within a 30-minute window for each fixed $1° \times 1°$ box. If the mean CF increase (decrease) more than 10%, clouds are classified as growing (dissipating). If the change in CF is less than 10%, clouds are classified as constant. Similar results are obtained using classification methods based on different CF thresholds (e.g., from 10% to 30%) or changes in the mean LWP (not shown).

As seen in Figures S4b, the LWP susceptibility for non-precipitating thin clouds in the growing or dissipating stages are similar or less negative than clouds that remain constant in CF. Additionally, the occurrence of dissipating and developing thin clouds remain relatively constant throughout the day (Fig. S4a), which differs from our hypothesis that thin clouds dissipate in the morning. Therefore, the decrease in LWP susceptibility in the morning is *unlikely* to be attributed to the dissipation or development of thin clouds. Yet, due to the observational limitation on estimating the mixing process from satellite retrievals, further investigation is needed to quantify the impact of cloud dissipation and the mixing type on the N_d-LWP relationship.

Hypothesis H2 is related to the response time of cloud LWP and CF to N_d perturbations. Both model simulations and observations have shown that the influence of aerosols on cloud LWP, achieved through adjusting the entrainment rate, may take four hours to become apparent and up to 20 hours to reach an equilibrium (Glassmeier et al. 2021; Gryspeerdt et al., 2021). Similarly, the impact of aerosols on CF may take approximately three to four hours to reach its maximum effect (Gryspeerdt et al., 2021). Therefore, during the diurnal transition of cloud state, clouds may still retain the " memory" of their susceptibilities from previous states, resulting in a diurnal variation in cloud susceptibility. This hypothesis is tested in Figure 5.

To quantify the dependence of current cloud susceptibility on previous cloud states, we track the cloud state for each $1° \times 1°$ box backward in time for two hours and classify the non-precipitating thin clouds into three groups (Fig. 5): (1) thin clouds that are currently classified as thin clouds and didn' t change states in the past two hours (thin → thin), (2) thin clouds that evolved from precipitating clouds (rain → thin), and (3) thin clouds that decayed from non-precipitating thick clouds (thick → thin). This backward tracking classification is applied at each time step.

As shown in Fig. 5a, at 9 LST, ~50% of the non-precipitating thin clouds originate from thick clouds in previous hours. The transition from thick to thin clouds is likely caused by the increased solar radiation after sunrise, leading to clouds decoupling from the ocean surface and a decrease in cloud LWP. In the evening, on the other hand, around 80% of the thin clouds are thin clouds in previous hours. In addition, less than 20% of the non-precipitating thin clouds are from precipitating clouds.

https://doi.org/10.5194/egusphere-2023-1676
Preprint. Discussion started: 23 August 2023

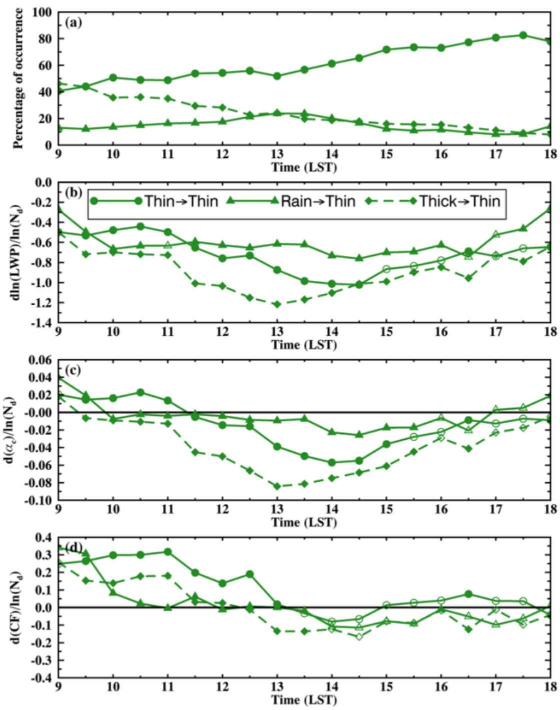

Figure 5. Daytime variation of non-precipitating thin clouds transition from non-precipitating thin clouds (thin → thin, solid line with circle symbols), precipitating clouds (rain → thin, solid line with triangle symbols), and non-precipitating thick clouds (thick → thin, dash line with diamond symbols) in previous two hours. Symbols for different state transitions are noted in (b). In (b)-(d), filled markers indicate data points that are significantly different from the other two groups (p<0.05), while open markers indicate statistical insignificance.

Non-precipitating thin clouds that are previously thick have significantly more negative LWP and α_c susceptibilities than thin clouds that are previously thin or precipitating (Figs. 5b and c). This difference is consistent with results shown in Fig. 2 between thick and thin clouds and could be attributed to the enhanced entrainment in the thick clouds. The differences among the three groups are more pronounced in the morning when a larger portion of thin clouds are decayed from thick clouds. In the afternoon, with less than 10% of thin clouds transitioning from thick or precipitating clouds, the differences among the three groups become less significant. These results support our hypothesis that clouds retain the memory of their responses to N_d perturbations from their previous states.

Similarly, responses of CF to N_d perturbations in the morning retain the memory of the previous state of clouds. As seen in Figure 5d, thin clouds that transitioned from thick clouds or precipitating clouds have significantly less positive CF susceptibility than thin clouds that are previously thin, particularly in the morning. This is likely due to the less positive CF susceptibility for non-precipitating thick and precipitating clouds in the morning, which will be discussed in section 3.4.2 and 3.4.3. In the afternoon, on the other hand, thin clouds transition from all three states have near-zero CF responses to N_d perturbations. Further analysis is required to explain this near-zero CF susceptibility in the afternoon.

The impact of the cloud memory of AIE on current cloud susceptibility is evident within a 30-minute window when a transition of cloud state just occurs (Fig. S5). Consistent with the findings in Figure 5, thin clouds that transition from thick clouds exhibit much more negative LWP and α_c susceptibilities compared to thin clouds that remain thin during the 30 minutes. However, due to the limited number of cases experiencing a transition in cloud state within a 30-miniute window (Fig. S5a), the differences in cloud susceptibilities between thin cloud undergoing a change in cloud states and those that do not are statistically

https://doi.org/10.5194/egusphere-2023-1676
Preprint. Discussion started: 23 August 2023

insignificant after 14 LST. In addition, the impact of the transition in cloud state on the current cloud susceptibility persists for at least four hours (Fig. S6). It is important to note that our tracking method does not follow individual cloud parcels to track changes in their states, and the influence of cloud advection may become more significant over longer tracking time, such as four hours. Therefore, a two-hour tracking window is used in this study.

In summary, the " U-shaped" diurnal variation in LWP and α_c susceptibilities for non-precipitating thin clouds are likely a combined effect of the transition in cloud state and cloud retaining the memory of AIE of their previous state. From morning to noon, as non-precipitating thick clouds transition to thin clouds, they retain their memory of the large negative LWP susceptibility. Therefore, both LWP and α_c susceptibilities decrease from morning to noon for thin clouds and reach their daily minima at noon. In the afternoon, as a growing percentage of thin clouds persist as thin clouds in previous hours, LWP and α_c susceptibilities gradually increase to less negative and near zero, respectively.

https://doi.org/10.5194/egusphere-2023-1676
Preprint. Discussion started: 23 August 2023

Table 1. Hypotheses for the diurnal variation of LWP and CF susceptibilities for warm boundary layer clouds.

Hypotheses	**Diurnal variation of LWP susceptibility**			**Diurnal variation of CF susceptibility**		
	Non-precipitating thin clouds	**Non-precipitating thick clouds**	**Precipitating clouds**	**Non-precipitating thin clouds**	**Non-precipitating thick clouds**	**Precipitating clouds**
H1. Changes in cloud morphology	N/A	N/A	N/A	N/A	Mostly overcast clouds in the morning and evening. CF of overcast clouds is less sensitive to N_d perturbations.	N/A
H2. LWP responses to N_d perturbations are slower than the state transition.	Non-precipitating thick clouds transition to thin clouds from morning to noon, which leads to a daily minimum LWP susceptibility at noon.	Thin clouds develop to thick clouds from noon to evening, which leads to an increase in LWP susceptibility.	Non-precipitating thin clouds transition to precipitating clouds in the afternoon, which leads to a decrease in LWP susceptibility.	Thick clouds transitioned to thin clouds from morning to noon, leading to a decrease in CF susceptibility	Cannot explain	Thin clouds transition to precipitating clouds in the afternoon, and lead to a decrease in CF susceptibility
H3. Dissipation or development of clouds	Cannot explain. Clouds that are growing or dissipating have similar LWP susceptibilities as clouds with constant CF.	Cannot explain.	Cannot explain.	Cannot explain.	Cannot explain.	Cannot explain

https://doi.org/10.5194/egusphere-2023-1676
Preprint. Discussion started: 23 August 2023

3.4.2 Non-precipitating thick clouds

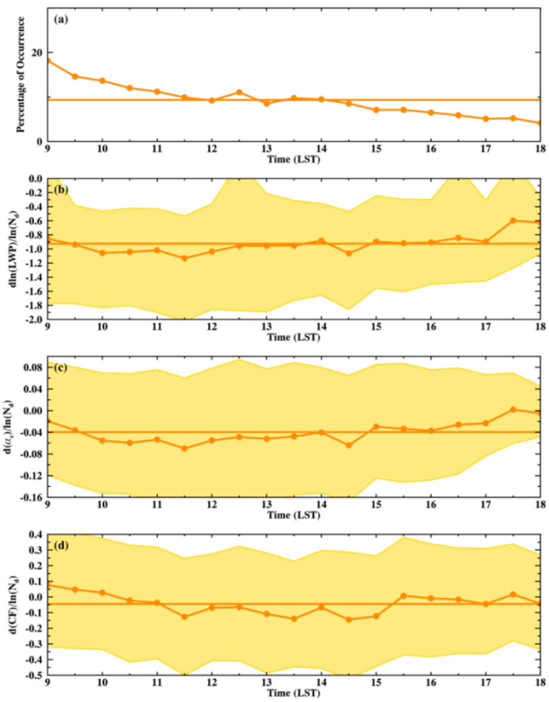

Figure 6. Daytime variation of (a) percentage of occurrence of non-precipitating thick clouds to warm boundary layer clouds, (b) cloud LWP susceptibility ($dln(LWP)/dln(N_d)$), (c) cloud albedo susceptibility ($d\alpha_c/dln(N_d)$), and (d) cloud fraction susceptibility ($dCF/dln(N_d)$) for non-precipitating thick clouds. The shaded areas represent the lower and upper 25th percentile of the cloud susceptibilities for each time step. The solid lines without symbols in (a)-(d) represent the daytime mean values.

Consistent with Fig. 2e, non-precipitating thick clouds are the least frequent warm boundary layer cloud state during summer over the ENA region. Their percentage of occurrence continuously decreases from 20% in the morning to less than 5% in the evening. As shown in Figs. 6b and c, the LWP and α_c susceptibilities for thick clouds first decrease from less negative to more negative in the morning and then increase from noon to evening. CF susceptibility is weakly positive in the early morning, becomes weakly negative from late morning to early afternoon, and increases to near zero in the evening (Fig. 6d). The diurnal variation of cloud susceptibilities for thick clouds is close to the cloud susceptibilities for thin clouds transition from thick clouds shown in Fig. 5d (thick → thin, dash line with diamond symbols), which supports our hypothesis on cloud retaining its memory of AIE of its previous cloud state.

To gain insight into the observed increase in LWP and α_c susceptibility from morning to evening, we investigate the influence of cloud state transition on cloud susceptibility for non-precipitating thick clouds (Figure 7), which is summarized as H2 in Table 1. As shown in Fig. 7a, around 40% of thick clouds sustain as thick clouds in previous two hours during the morning period; whereases during the late afternoon to evening, with decreasing solar radiation, more than 60% of thick clouds are developed from thin clouds in previous two hours. Consistent with the findings presented in Fig. 5, thick clouds that are previously thick exhibit significantly more negative LWP susceptibility compared to thick clouds that are previously thin (Fig. 7b). These differences are particularly prominent in the morning. However, as the total percentage of thick clouds decrease to less than 10% in the afternoon (Fig. 6a), the limited number of samples for all three groups results in non-significant differences

https://doi.org/10.5194/egusphere-2023-1676
Preprint. Discussion started: 23 August 2023

in LWP susceptibility among them. Additionally, Fig. 7d indicates that transition in cloud state cannot account for the diurnal variation in CF susceptibility for thick clouds, as all three groups are insignificantly different from each other.

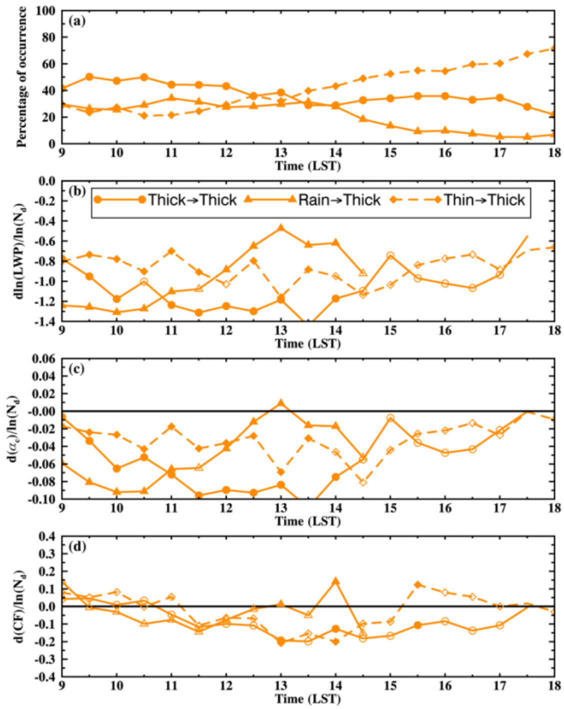

Figure 7. Daytime variation of non-precipitating thick clouds transition from non-precipitating thick clouds (thick → thick, solid line with circle symbols), precipitating clouds (rain → thick, solid line with triangle symbols), and non-precipitating thin clouds (thin → thick, dash line with diamond symbols) in previous two hours. Symbols for different state transitions are noted in (b). In (b)-(d), filled markers indicate data points that are significantly different from the other two groups (p<0.05), while open markers indicate statistical insignificance.

To understand the driving force for the diurnal variation in CF susceptibility shown in Figure 6d, we calculate the mean cloud properties for non-precipitating thin and thick clouds, as shown in Figure S3. In the morning, non-precipitating thick clouds are predominantly overcast clouds with a mean CF of 75% (Fig. S3a). To distinguish between overcast and broken clouds, we calculate the diameter-to-height ratio (DHR) for each cloud, where diameter is estimated by the square root of the area and height is defined as the 90th percentile of cloud tops. As shown in Fig. S3c, thick clouds are mostly overcast in the morning with a mean DHR of 230. Compared to broken clouds, overcast clouds have less room for CF to increase, which results in a less positive CF susceptibility for thick clouds compare to thin CF. After 10 am, non-precipitating thick clouds start to break. The mean CF decreases from 75% at 10 am to 60% at 2 pm and the DHR decreases from 230 to 170. As CF for broken clouds is more sensitive to N_d perturbations, CF susceptibility decreases to $-0.13\ ln(N_d)^{-1}$, which is consistent with the daytime mean negative CF susceptibility shown in Fig.2c. From afternoon to evening, clouds transition to overcast again (Fig. S3), and the CF susceptibility increases back to zero. This impact of cloud morphology (e.g., overcast or broken clouds) on diurnal variation of CF susceptibility is summarized as H1 in Table 1.

In conclusion, LWP susceptibility for non-precipitating thick clouds first decrease from less negative to more negative in the morning and then increase from noon to evening, which is likely attributed to the transition from thin to thick clouds. In the morning, 40% to 50% of thick clouds are previously thick clouds, these clouds exhibit a large negative LWP susceptibility. In the afternoon, 60-70% of thick clouds develop from thin clouds in previous hours and retain the memory of LWP

https://doi.org/10.5194/egusphere-2023-1676
Preprint. Discussion started: 23 August 2023

susceptibility of thin clouds. Therefore, LWP susceptibility increases in the afternoon, and become similar to that of thin clouds (Fig. 4b, 6b). Diurnal variation in CF susceptibility for thick clouds is likely attributed to changes in cloud morphology. In the morning and evening, thick clouds are mostly overcast with CF less sensitive to N_d perturbations, resulting in a near zero CF susceptibility. From late morning to early afternoon, the overcast thick clouds break down and CF decrease with increasing N_d due to the enhanced entrainment and evaporation.

The impact of cloud memory and transition of cloud state on the diurnal variation of LWP susceptibility is summarized as a schematic figure shown in Figure 8. From morning to noon, as non-precipitating thick clouds transition to thin clouds, they retain their memory of the large negative LWP susceptibility. Therefore, LWP susceptibility for thin clouds reach its daily minima in the early afternoon. From early afternoon to evening, with non-precipitating thin clouds developing to thick clouds, LWP susceptibility for thick clouds increase.

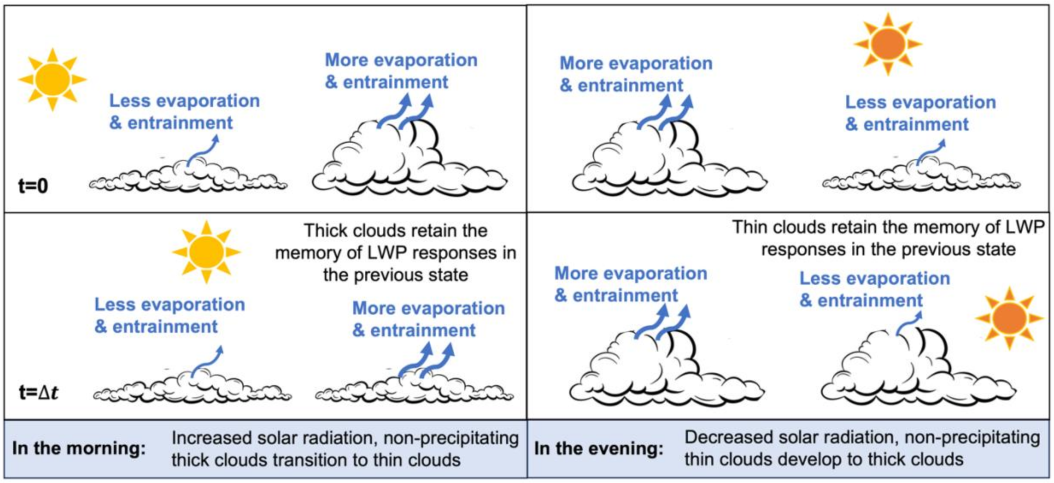

Figure 8. Schematic figure of influence of cloud memory and transition of cloud state on the LWP susceptibility and its diurnal variation.

3.4.3 Precipitating clouds

As shown in Figure 9a, precipitating clouds are the dominant cloud state in this region, accounting for 46% of the warm boundary layer clouds, compared to 44% of non-precipitating thin clouds. The frequency of precipitating clouds is higher in the morning and evening compared to noon. Throughout the day, the mean LWP susceptibility remain consistently negative, fluctuating between −0.5 to −0.3, with minimum values between 14–16 LST (Fig. 9b). The diurnal variability in LWP susceptibility for precipitating clouds is much lower than that for non-precipitating thin (e.g., from −0.9 to −0.4) and thick (e.g., from −1.1 to −0.6) clouds. The negative LWP susceptibility is likely due to the prevalence of lightly precipitating clouds, with a mean precipitating fraction ranging from 0.2 to 0.5 (Fig. S2d). The influence of precipitation suppression is smaller than that of the entrainment enhancement. Similarly, α_c susceptibility fluctuates between 0 to 0.02 throughout the day, with near zero α_c susceptibility in early afternoon (Fig. 9c). Despite the minimal diurnal variation, the LWP and α_c susceptibilities at 13-16 LST are statistically significant different than cloud susceptibilities in the morning and evening at 95% confidence level with the two-tailed t-test. The CF susceptibility for precipitating clouds also shows minimal diurnal variation compared to non-precipitating clouds, with a mean value ranging from 0 to 0.1 (Fig. 9d).

https://doi.org/10.5194/egusphere-2023-1676
Preprint. Discussion started: 23 August 2023

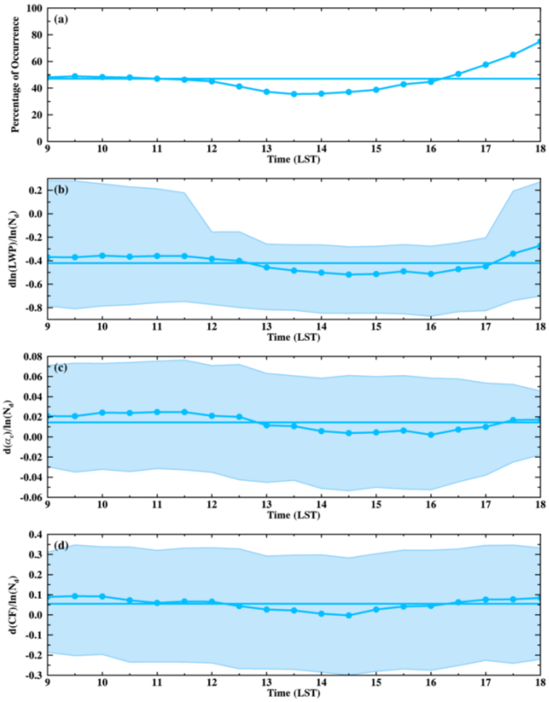

Figure 9. Daytime variation of (a) percentage of occurrence of precipitating clouds to warm boundary layer clouds, (b) cloud LWP susceptibility ($dln(LWP)/dln(N_d)$), (c) cloud albedo susceptibility ($d\alpha_c/dln(N_d)$), and (d) cloud fraction susceptibility ($dCF/dln(N_d)$) for precipitating clouds. The shaded areas represent the lower and upper 25th percentile of the cloud susceptibilities for each time step. The solid lines without symbols in (a)-(d) represent the daytime mean values.

Consistent with non-precipitating clouds, the diurnal variation of LWP and α_c susceptibilities for precipitating clouds can be attributed to the transition of cloud states. For example, as shown in Figure 10b-d, precipitating clouds that transition from non-precipitating thin clouds exhibit significantly more negative/less positive cloud susceptibilities than precipitating clouds that are previously precipitating. Meanwhile, α_c and CF susceptibilities switch signs from positive to negative in the afternoon for precipitating clouds transition from non-precipitating thin clouds compared to that are previously precipitating. Starting from 13 LST, when non-precipitating thin clouds transition to precipitating clouds (Fig. 10a), LWP and α_c susceptibilities begin to decrease and reach their daily minimum in the late afternoon. Interestingly, as non-precipitating thin clouds transition to precipitating clouds (Fig. 10b and c, thin → rain), their LWP and α_c susceptibilities exhibit both less negative values and smaller diurnal variations compared to thin clouds that remain as thin (Fig. 5b and c, thin → thin). The underlying reason for this observation is currently unclear and worth further investigations. Furthermore, the percentage of precipitating clouds that transition from non-precipitating thick clouds is less than 7% (Fig. 10a). Due to the limited number of cases, precipitating clouds that evolve from non-precipitating thick clouds do not exhibit significantly more negative LWP susceptibilities, especially during the period from 11 to 14 LST when the transition percentage decreases to 3%.

https://doi.org/10.5194/egusphere-2023-1676
Preprint. Discussion started: 23 August 2023

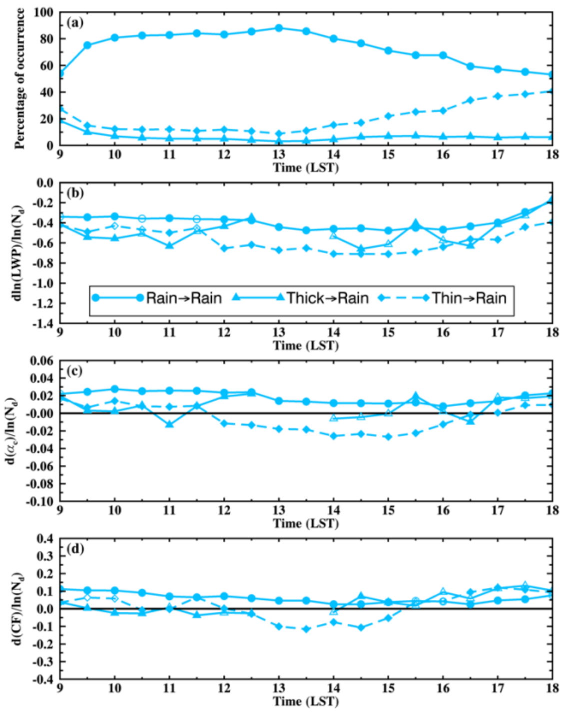

Figure 10. Daytime variation of precipitating clouds transitioned from precipitating clouds (rain → rain, solid line with circle symbols), non-precipitating thick clouds (thick → rain, solid line with triangle symbols), and non-precipitating thin clouds (thin → rain, dash line with diamond symbols) in previous two hours. Symbols for different state transitions are noted in (b). In (b)-(d), filled markers indicate data points that are significantly different from the other two groups (p<0.05), while open markers indicate statistical insignificance.

In conclusion, precipitating clouds exhibit smaller diurnal variation in cloud susceptibilities compared to non-precipitating thin and thick clouds. The decrease of LWP and α_c susceptibilities for precipitating clouds in the afternoon is likely contributed by the transition of non-precipitating thin clouds to precipitating clouds.

Combining the results shown here and results in section 3.4.1, we can answer the question raised in section 3.3. The non-precipitating thin clouds exhibit similar diurnal variation in LWP, α_c, and CF susceptibility as the warm boundary layer clouds with clouds being less susceptible to N_d perturbations in the morning and evening and more susceptible at noon. Additionally, non-precipitating thin clouds have highest frequency at noon. On the other hand, precipitating clouds, despite their higher percentage of occurrence than thin clouds, exhibit minimal diurnal variation in cloud susceptibility. Therefore, the pronounced diurnal variations in cloud susceptibilities for warm boundary layer clouds primarily stem from non-precipitating thin clouds.

3.5 Contribution to the diurnal variation of cloud susceptibility

As discussed in the previous section, both the frequency of occurrence of cloud states and the intensity of cloud responses to N_d perturbations show strong diurnal variations. In this section, we aim to compare the contribution of these two components to the overall diurnal variation in cloud susceptibilities by fixing one component constant at a time. The contribution from changes in the frequency of cloud states is represented by the red lines in Fig.11, which is estimated by weighting the daytime mean cloud susceptibility (Figs. 2a-c) with the half-hourly frequency of occurrence of clouds in the LWP-N_d parameter space, assuming a constant intensity of AIE during the daytime. The contribution from changes in the AIE intensity is depicted

https://doi.org/10.5194/egusphere-2023-1676
Preprint. Discussion started: 23 August 2023

by the blue lines, which is estimated by weighting the half-hourly cloud susceptibility in the LWP-N_d parameter space with the daytime mean frequency of occurrence of clouds (Fig. 2e), assuming a constant frequency during the daytime. The black line in Fig. 11 represents the observed susceptibility which considers the diurnal variations in both components.

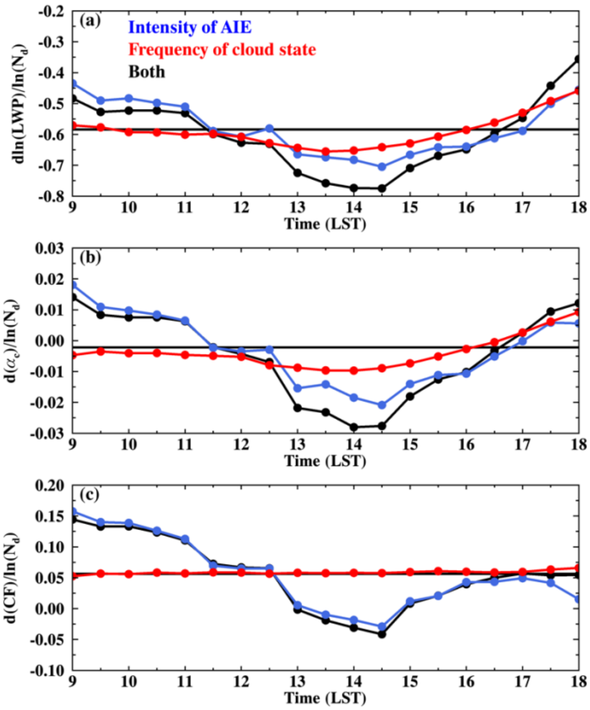

Figure 11. Daytime variation in cloud susceptibility contributed from the variability in the intensity of susceptibility (blue lines with symbols), variability in the frequency of occurrence of cloud state (red lines with symbols), and from both (black lines with symbols). (a) cloud LWP susceptibility ($dln(LWP)/dln(N_d)$), (b) cloud albedo susceptibility ($d\alpha_c/dln(N_d)$), (c) cloud fraction susceptibility ($dCF/dln(N_d)$). The black solid lines without symbols in (a)-(c) are the daytime mean susceptibility.

When comparing the net observed diurnal variation of cloud susceptibilities (black lines) with the contributions from changes in the intensity of AIE and the frequency of cloud state (blue and red lines, respectively), we find that the diurnal changes in cloud susceptibility is primarily driven by changes in the intensity of AIE during the day. This is especially evident for CF susceptibility, where the blue line closely represents the actual diurnal variation as indicated by the black line. Additionally, as shown in Figs. 11a and b, the red lines are close to the daytime mean values in the morning, which indicates that variations in the frequency of different cloud states have minimal impact on changes in LWP and α_c susceptibilities in the morning. On the other hand, in the afternoon, both shifts in cloud states and changes in intensities contribute to the changes in LWP and α_c susceptibilities.

In summary, since polar-orbiting satellites can only observe the intensity of AIE across different cloud states at their overpass time, they cannot fully capture the diurnal variation of cloud susceptibilities driven by the diurnal variation in AIE intensity. Given that all three cloud susceptibilities reach their daily minimum at around 13:30 LST, studies based on polar-orbiting satellite with overpass time at noon may be underestimating the daily mean value of cloud susceptibility.

https://doi.org/10.5194/egusphere-2023-1676
Preprint. Discussion started: 23 August 2023

4. Discussions

In this study, we quantify the instantaneous responses of warm boundary layer clouds to N_d perturbation using the pixel-level SEVIRI cloud retrievals of each time step. For heavily precipitating clouds, LWP increases under pristine condition (e.g., N_d < 30 cm^{-3}, Fig. 2a). For lightly precipitating and non-precipitating clouds, LWP decreases with N_d. The N_d-LWP relationship find in this study is consistent with that in Gryspeerdt et al. (2019) using global mean cloud retrievals from MODIS and AMSR-E at coarser resolution of 1° × 1° and daily timescale. This consistency between different satellite measurements at different temporal and spatial scales greatly enhance our confidence in the retrieved relationship.

This study further distinguishes non-precipitating clouds into thin and thick clouds based on their LWP. A consistent decreasing trend in cloud water is found for both states, yet non-precipitating thick clouds exhibit more negative LWP susceptibility ($\frac{dln(LWP)}{dln(N_d)} = -0.94$) compared to thin clouds ($\frac{dln(LWP)}{dln(N_d)} = -0.71$). The LWP susceptibilities estimated in this study are more negative than those in Zhang et al. (2022) and Zhang and Feingold (2023), based on similar classification of cloud states. Particularly, we found that non-precipitating thin clouds have a decreasing trend in cloud water and a warming effect on the surface radiation while these are opposite in Zhang et al. (2022) and Zhang and Feingold (2023). We speculate this difference is due to the less stable troposphere, deeper boundary layer, and the higher cloud tops over the ENA regions (e.g., Klein and Hartmann, 1993; Ding et al., 2021; King et al., 2013) compared to the NE Pacific in Zhang et al. (2022) and the study regions in Zhang and Feingold (2023). The less stable condition over the studied region leads to a deeper boundary layer, deeper clouds, and a stronger entrainment rate at the cloud top, all of which may cause a more negative LWP susceptibility (Possner et al., 2020; Toll et al., 2019).

Regarding the CF adjustment to N_d perturbation, a daytime mean positive response is found for precipitating and non-precipitating thin clouds and a negative response for non-precipitating thick clouds (Fig. 2c). Few studies have quantified the instantaneous CF adjustment rate for a directly comparison of CF susceptibility. However, similar results are found using measurement and retrievals from different platforms at various timescales, which greatly increase our confidence in the observed CF responses toward N_d perturbation. For example, using MODIS measurement, Kaufman et al. (2005) found an increase in the longitudinal mean cloudiness for warm boundary layer clouds with increasing AOD in all four regions of the Atlantic Ocean characterized by distinct aerosol types. Using the natural experiment of volcanic eruption at Holuhraun in Iceland, Chen et al. (2022) found that aerosols from the eruption increase the monthly mean cloud cover by 10% over the North Atlantic. By tracking the cloud trajectory using geostationary satellite, Christensen et al. (2020) found that aerosol enhance both CF and cloud lifetime in the timescale of 2-3 days, especially under stable conditions. It is worth noting that a decrease in CF was not observed in these studies, likely due to the prevalence of non-precipitating thin clouds and precipitating clouds in the Atlantic or the NE Pacific (e.g., Zhang and Feingold, 2023) that mask the signal from non-precipitating thick clouds without distinguishing cloud states.

5. Conclusions

Using N_d as an intermediary variable, this study investigates the aerosol indirect effect (AIE) and its diurnal variation over the ENA region with half-hourly and 3-km cloud property retrievals from SEVIRI on the Meteosat-11. To constrain meteorological impacts on clouds and aerosol-cloud interaction, cloud susceptibilities are estimated within a 1° × 1° grid box for each satellite time step. Based on the daytime mean cloud susceptibilities in the LWP-N_d parameter space, the sign and magnitude of cloud susceptibilities strongly depend on the cloud states (Fig. 2).

https://doi.org/10.5194/egusphere-2023-1676
Preprint. Discussion started: 23 August 2023

Precipitating clouds exhibit contrasting responses in cloud LWP, with increases observed for heavily precipitating clouds and decreases for lightly precipitating clouds. Positive α_c and CF susceptibilities are identified for both heavily and lightly precipitating clouds. The net radiative forcing of the AIE on precipitating clouds is estimated to be $-13\ W\ m^{-2} ln(N_d)^{-1}$, with contributions from the CF and α_c effects of -9.5 and $-3.5\ W\ m^{-2}\ ln(N_d)^{-1}$, respectively.

For non-precipitating clouds, LWP susceptibility becomes more negative with increasing LWP and N_d, likely due to the enhanced entrainment leading to stronger evaporation and reductions in LWP with increased N_d. Consistent with the evaporation-entrainment feedback hypothesis, non-precipitating thick clouds exhibit decreasing CF and α_c with increasing N_d, and have a net radiative forcing of $+4.4\ W\ m^{-2}\ ln(N_d)^{-1}$. On the other hand, non-precipitating thin clouds show weaker LWP and α_c responses and an increasing response in CF. The increase in CF compensates for the decrease of α_c and leads to a net cooling effect of $-4.3\ W\ m^{-2}\ ln(N_d)^{-1}$.

Warm boundary layer clouds exhibit strong and significant ($p<0.05$) diurnal variations in cloud susceptibilities, with all three cloud susceptibilities exhibiting "U-shaped" diurnal patterns where susceptibilities are lowest during the early afternoon (Fig. 3). Meanwhile, there is little spatial variability in cloud susceptibilities in the study region and the diurnal cycle of cloud susceptibility over the $1° \times 1°$ box at the ARM ENA site agree well with the domain mean value, which imply the regional representativeness of the ARM ENA site of AIE. Based on our analysis of the diurnal variation of cloud susceptibility for different cloud states (Figs. 4, 6, 9), we find that the diurnal variations in cloud susceptibilities for all warm boundary layer clouds are primarily driven by non-precipitating thin clouds. They have similar "U-shaped" diurnal patterns in cloud susceptibilities and constitute approximately 44% of the warm boundary layer clouds in this region (Fig. 4).

Diurnal variation in LWP and α_c susceptibilities for non-precipitating thin clouds is likely due to the combined effect of transition in cloud state and the slower response of clouds to N_d perturbation than the satellite timescale (H2 in Table 1). As non-precipitating clouds transition from thick to thin, the "memory" of LWP responses to N_d perturbations is retained. Consequently, the LWP susceptibility for thin clouds transition from thick clouds is 0.2-0.4 more negative compared to those that are previously thin clouds, which accounts for 40-60% of the observed changes (Fig. 5). The differences are larger in the morning when cloud state transitions are more frequent. Similarly, non-precipitating thick clouds that develop from thin clouds in previous hours exhibit 0.2-0.5 less negative LWP susceptibility than thick clouds that remain consistently thick (Fig. 7). Meanwhile, diurnal variation in CF susceptibility for non-precipitating thick clouds is more likely driven by changes in cloud morphology rather than the transition of cloud state (Fig. S3, H1 in Table 1). Compared to non-precipitating clouds, precipitating clouds exhibit smaller diurnal variation in cloud susceptibility (Fig. 9). The decrease of cloud susceptibility for precipitating clouds in the afternoon is likely attributed to the transition of non-precipitating thin clouds to precipitating clouds. (Fig. 10).

The diurnal variation in cloud susceptibility is primarily driven by changes in the intensity of AIE from morning to noon, rather than changes in the frequency of occurrence of different cloud states (Fig. 11). As the polar-orbiting satellites only observe cloud susceptibilities across different cloud states during a specific overpass time, and all three cloud susceptibilities reach their daily minimum at noon. Based on the estimated diurnal variation, using satellite retrievals at 13:30 LST could underestimate the daytime mean value of LWP susceptibility by 26.3% (-0.76 compared to -0.60), the α_c susceptibility by 475% (-0.023 compared to -0.004), and the CF susceptibility by 120% (-0.019 compared to $+0.055$).

This study underscores the importance of considering the diurnal cycle of cloud susceptibilities when quantifying AIE and their impacts on clouds and radiation. The classification of cloud states enables us to distinguish the sign, magnitude, and underlying processes driving the diurnal variation of AIE.

To further advance our understanding of the diurnal variation of AIE, several avenues for future research can be pursued. Firstly, it is important to address uncertainties associated with satellite retrievals, which can propagate into uncertainties in the retrieved N_d, as discussed in Grosvenor et al. (2018). Future study could utilize active sensors to reduce these uncertainties, particularly during nighttime conditions. Moreover, using the retrieved N_d as a proxy of aerosol concentration may introduce uncertainties related to cloud processes that can act as sources or sinks of N_d, potentially buffer the relationships between N_d and cloud condensation nuclei. Future investigations are needed to better understand the relationships, and how they vary with different cloud processes and throughout the day. Lastly, this study encompasses all warm boundary layer clouds without considering the highly diverse meteorological regimes and cloud types in the ENA region. Classification of the synoptic and meteorological conditions associated with different cloud states and aerosol properties would contribute to a more comprehensive understanding, allowing for the disentanglement of the impacts of meteorology from AIE.

Data availability:

SEVIRI Meteosat-11 cloud retrieval products, produced by NASA LaRC SatCORPS group, are available from the Atmospheric Radiation Measurement (ARM) Data Discovery website at https://adc.arm.gov/discovery/, Minnis Cloud Products Using Visst Algorithm (visstgridm11minnis). The ARM ground-based radar and lidar observations are available from ARM Data Discovery, KAZRARSCL, (arsclkazr1kollias).

Acknowledgment:

We are grateful to the Atmospheric Radiation Measurement (ARM) user facility, a U.S. Department of Energy (DOE) Office of Science user facility managed by the Biological and Environmental Research Program for providing ARM observation data and archiving SEVIRI Meteosat-11 cloud retrieval products. We mainly used the computing resources from the National Energy Research Scientific Computing Center (NERSC), which is supported by the Office of Science of the U.S. Department of Energy under Contract No. DE-AC02-05CH11231. This work was performed under the auspices of the U.S. DOE by LLNL under contract DE-AC52-07NA27344. (LLNL-JRNL-851496)

Financial support:

This work is supported by the DOE Office of Science Early Career Research Program and the ASR Program. DP acknowledges the support of the NASA CloudSat CALIPSO Science Recompete Program.

Competing interests:

The authors declare that they have no conflict of interest.

References

Albrecht, B. A.: Aerosols, Cloud Microphysics, and Fractional Cloudiness, Science, 245, 1227–1230, https://doi.org/10.1126/science.245.4923.1227, 1989.

Bennartz, R.: Global assessment of marine boundary layer cloud droplet number concentration from satellite, J. Geophys. Res.,112, D02201, doi:10.1029/2006JD007547, 2007.

Bennartz, R. and Rausch, J.: Global and regional estimates of warm cloud droplet number concentration based on 13 years of AQUA-MODIS observations, Atmos. Chem. Phys., 17, 9815–9836, https://doi.org/10.5194/acp-17-9815-2017, 2017.

Bréon, F.-M., Tanré, D., and Generoso, S.: Aerosol effect on cloud droplet size monitored from satellite, Science, 295, 834–838, 2002.

Bretherton, C. S., Blossey, P. N., and Uchida, J.: Cloud droplet sedimentation, entrainment efficiency, and subtropical stratocumulus albedo, Geophys. Res. Lett., 34, L03813, https://doi.org/10.1029/2006GL027648, 2007.

Brenguier, J. L., Burnet, F., & Geoffroy, O.: Cloud optical thickness and liquid water path – does the coefficient vary with droplet concentration? *Atmospheric Chemistry and Physics*, *11*(18), 9771-9786. https://doi.org/10.5194/acp-11-9771-2011, 2011

Chen, Y.-C., Christensen, M., Stephens, G. L., and Seinfeld, J. H.: Satellite-based estimate of global aerosol–cloud radiative forcing by marine warm clouds, Nature Geosci., 7, 643–646, https://doi.org/10.1038/ngeo2214, 2014.

Chen, Y., Haywood, J., Wang, Y., Malavelle, F., Jordan, G., Partridge, D., Fieldsend, J., De Leeuw, J., Schmidt, A., Cho, N., Oreopoulos, L., Platnick, S., Grosvenor, D., Field, P., & Lohmann, U.: Machine learning reveals climate forcing from aerosols is dominated by increased cloud cover. *Nature Geoscience*, *15*(8), 609-614, 2022. https://doi.org/10.1038/s41561-022-00991-6

Christensen, M. W., Jones, W. K., and Stier, P.: Aerosols enhance cloud lifetime and brightness along the stratus-tocumulus transition, P. Natl. Acad. Sci. USA, 117, 17591–17598, https://doi.org/10.1073/pnas.1921231117, 2020.

Comstock, K. K., Wood, R., Yuter, S. E., and Bretherton, C. S.: Reflectivity and rain rate in and below drizzling stratocumulus, Q. J. Roy. Meteorol. Soc., 130, 2891–2918, doi:10.1256/qj.03.187, 2004.

Ding, F., Iredell, L., Theobald, M., Wei, J., & Meyer, D. :. PBL Height From AIRS, GPS RO, and MERRA-2 Products in NASA GES DISC and Their 10-Year Seasonal Mean Intercomparison. *Earth and Space Science*, *8*(9). https://doi.org/10.1029/2021ea001859, 2021

Dong, X., Xi, B., Kennedy, A., Minnis, P., & Wood, R.: A 19-month record of marine aerosol–cloud–radiation properties derived from DOE ARM mobile facility deployment at the Azores. Part I: Cloud fraction and single-layered MBL cloud properties. Journal of Climate, 27(10), 3665–3682. https://doi.org/10.1175/JCLI-D-13-00553.1, 2014.

Dong, X., Xi, B., Qiu, S., Minnis, P., Sun-Mack, S., & Rose, F. : A radiation closure study of Arctic stratus cloud microphysical properties using the collocated satellite-surface data and Fu-Liou radiative transfer model. *Journal of Geophysical Research: Atmospheres*, *121*(17), 10,175-110,198. https://doi.org/10.1002/2016jd025255, 2016

Dong, X., Zheng, X., Xi, B., & Xie, S.: A Climatology of Midlatitude Maritime Cloud Fraction and Radiative Effect Derived from the ARM ENA Ground-Based Observations. Journal of Climate, 36(2), 531–546, https://doi.org/10.1175/JCLI-D-22-0290.1, 2023.

Duong, H. T., Sorooshian, A., and Feingold, G.: Investigating potential biases in observed and modeled metrics of aerosol-cloud precipitation interactions, Atmos. Chem. Phys., 11, 4027–4037, doi:10.5194/acp-11-4027-2011, 2011.

Fan, J. W., Wang, Y., Rosenfeld, D., and Liu, X. H.: Review of aerosol-cloud interactions: mechanisms, significance, and challenges, J. Atmos. Sci., 73, 4221–4252, 2016.

https://doi.org/10.5194/egusphere-2023-1676
Preprint. Discussion started: 23 August 2023

Feingold G, Eberhard W, Veron D, Previdi M. First measurements of the Twomey indirect effect using ground-based remote sensors. Geophys Res Lett. 30 (6). https://doi.org/10.1029/2002GL016633, 2003.

Glassmeier, F., Hoffmann, F., Johnson, J. S., Yamaguchi, T., Carslaw, K. S., and Feingold, G.: Aerosol-cloud-climate cooling overestimated by ship-track data, Science, 371, 485–489, https://doi.org/10.1126/science.abd3980, 2021.

Grosvenor, D. P., & Wood, R.: The effect of solar zenith angle on MODIS cloud optical and microphysical retrievals within marine liquid water clouds. *Atmospheric Chemistry and Physics*, *14*(14), 7291-7321. https://doi.org/10.5194/acp-14-7291-2014, 2014

Grosvenor, D. P., Sourdeval, O., Zuidema, P., Ackerman, A., Alexandrov, M. D., Bennartz, R., Boers, R., Cairns, B., Chiu, J. C., Christensen, M., Deneke, H., Diamond, M., Feingold, G., Fridlind, A., HÃOEnerbein, A., Knist, C., Kollias, P., Marshak, A., McCoy, D., Merk, D., Painemal, D., Rausch, J., Rosenfeld, D., Russchenberg, H., Seifert, P., Sinclair, K., Stier, P., van Diedenhoven, B., Wendisch, M., Werner, F., Wood, R., Zhang, Z., and Quaas, J.: Remote Sensing of Droplet Number Concentration in Warm Clouds: A Review of the Current State of Knowledge and Perspectives, Rev. Geophys., 56, 409–453, https://doi.org/10.1029/2017RG000593, 2018.

Gryspeerdt, E., Quaas, J., and Bellouin, N.: Constraining the aerosol influence on cloud fraction, J. Geophys. Res.-Atmos., 121, 3566– 3583, https://doi.org/10.1002/2015JD023744, 2016.

Gryspeerdt, E., Goren, T., Sourdeval, O., Quaas, J., Mülmenst.dt, J., Dipu, S., Unglaub, C., Gettelman, A., and Christensen, M.: Constraining the aerosol influence on cloud liquid water path, Atmos. Chem. Phys., 19, 5331–5347, https://doi.org/10.5194/acp-19-5331-2019, 2019.

Gryspeerdt, E., Goren, T., and Smith, T. W. P.: Observing the timescales of aerosol–cloud interactions in snapshot satellite images, Atmos. Chem. Phys., 21, 6093–6109, https://doi.org/10.5194/acp-21-6093-2021, 2021.

Gryspeerdt, E., McCoy, D. T., Crosbie, E., Moore, R. H., Nott, G. J., Painemal, D., Small-Griswold, J., Sorooshian, A., and Ziemba, L.: The impact of sampling strategy on the cloud droplet number concentration estimated from satellite data, Atmos.Meas. Tech., 15, 3875–3892, https://doi.org/10.5194/amt-15-3875-2022, 2022.

Han, Q., Rossow, W. B., Zeng, J., and Welch, R.: Three Different Behaviors of Liquid Water Path of Water Clouds in Aerosol–Cloud Interactions, J. Atmos. Sci., 59, 726–735, https://doi.org/10.1175/1520-0469(2002)059<0726:TDBOLW>2.0.CO;2, 2002.

Kaufman, Y. J., Koren, I., Remer, L. A., Rosenfeld, D., & Rudich, Y.: The effect of smoke, dust, and pollution aerosol on shallow cloud development over the Atlantic Ocean. *Proc Natl Acad Sci U S A*, *102*(32), 11207-11212. https://doi.org/10.1073/pnas.0505191102, 2005

King, M. D., Platnick, S., Menzel, W. P., Ackerman, S. A., & Hubanks, P. A.: Spatial and Temporal Distribution of Clouds Observed by MODIS Onboard the Terra and Aqua Satellites. *IEEE Transactions on Geoscience and Remote Sensing*, *51*(7), 3826-3852. https://doi.org/10.1109/tgrs.2012.2227333, 2013

Klein, S. A., & Hartmann, D. L.: The seasonal cycle of low stratiform clouds. Journal of Climate, 6(8), 1587–1606. https://doi.org/10.1175/1520-0442(1993)006<1587:tscols>2.0.co;2, 1993

Mather, J. H., & Voyles, J. W.: The Arm Climate Research Facility: A Review of Structure and Capabilities, *Bull. Am. Meteorol. Soc.*, 94, 377-392, https://doi.org/10.1175/BAMS-D-11- 00218.1, 2013.

Mechem, D. B., Wittman, C. S., Miller, M. A., Yuter, S. E., and De Szoeke, S. P.: Joint synoptic and cloud variability over the Northeast Atlantic near the Azores, J. Appl. Meteorol. Clim., 57, 1273–1290, 2018.

Minnis, P., Sun-Mack, S., Young, D. F., Heck, P. W., Garber, D. P., Chen, Y., Spangenberg, D. A., Arduini, R. F., Trepte, Q. Z., Smith, W. L., Ayers, J. K., Gibson, S. C., Miller, W. F., Hong, G., Chakrapani, V., Takano, Y., Liou, K., Xie, Y., and Yang,

https://doi.org/10.5194/egusphere-2023-1676
Preprint. Discussion started: 23 August 2023

P.: CERES edition-2 cloud property retrievals using TRMM VIRS and Terra and Aqua MODIS data–Part I: Algorithms, IEEE Trans. Geosci. Remote Sens., 49, 4374–4400, https://doi.org/10.1109/TGRS.2011.2144601, 2011.

Minnis, P., K. Bedka, Q. Trepte, C. R. Yost, S. T. Bedka, B. Scarino, K. Khlopenkov, and M. M. Khaiyer: A consistent long-term cloud and clear-sky radiation property dataset from the Advanced Very High Resolution Radiometer (AVHRR). Climate Algorithm Theoretical Basis Document (C-ATBD), CDRP-ATBD-0826 Rev 1 - NASA, NOAA CDR Program, 159 pp., DOI:10.789/V5HT2M8T, https://www1.ncdc.noaa.gov/pub/data/sds/cdr/CDRs/AVHRR_Cloud_Properties_NASA/AlgorithmDescription_01B-30b.pdf, 2016.

Minnis, P., Sun-Mack, S., Chen, Y., Chang, F., Yost, C. R., Smith, W. L., Heck, P. W., Arduini, R. F., Bedka, S. T., Yi, Y., Hong, G., Jin, Z., Painemal, D., Palikonda, R., Scarino, B. R., Spangenberg, D. A., Smith, R. A., Trepte, Q. Z., Yang, P., and Xie, Y.: CERES MODIS Cloud Product Retrievals for Edition 4–Part I: Algorithm Changes, IEEE T. Geosci. Remote, 11152, 1–37, https://doi.org/10.1117/12.2532931, 2020.

Morrison, H., van Lier-Walqui, M., Fridlind, A. M., Grabowski, W. W., Harrington, J. Y., Hoose, C., et al.: Confronting the challenge of modeling cloud and precipitation microphysics. Journal of Advances in Modeling Earth Systems, 12, e2019MS001689. https://doi.org/10.1029/2019MS001689, 2020.

Painemal, D., Minnis, P., and Sun-Mack, S.: The impact of horizontal heterogeneities, cloud fraction, and liquid water path on warm cloud effective radii from CERES-like Aqua MODIS retrievals, Atmos. Chem. Phys., 13, 9997–10003, https://doi.org/10.5194/acp-13-9997-2013, 2013.

Painemal, D.: Global Estimates of Changes in Shortwave Low-Cloud Albedo and Fluxes Due to Variations in Cloud Droplet Number Concentration Derived From CERES-MODIS Satellite Sensors, Geophys. Res. Lett., 45, 9288–9296, https://doi.org/10.1029/2018GL078880, 2018.

Painemal, D., Spangenberg, D., Smith Jr.,W. L., Minnis, P., Cairns, B., Moore, R. H., Crosbie, E., Robinson, C., Thornhill, K. L., Winstead, E. L., and Ziemba, L.: Evaluation of satellite retrievals of liquid clouds from the GOES-13 imager and MODIS over the midlatitude North Atlantic during the NAAMES campaign, Atmos. Meas. Tech., 14, 6633–6646, https://doi.org/10.5194/amt-14-6633-2021, 2021.

Penner, J. E., Dong, X., and Chen, Y.: Observational evidence of a change in radiative forcing due to the indirect aerosol effect, Nature, 427, 231–234, 2004.

Possner, A., Eastman, R., Bender, F., & Glassmeier, F.: Deconvolution of boundary layer depth and aerosol constraints on cloud water path in subtropical stratocumulus decks. *Atmospheric Chemistry and Physics*, *20*(6), 3609-3621. https://doi.org/10.5194/acp-20-3609-2020, 2020

Rémillard, J., Kollias, P., Luke, E., and Wood, R.: Marine Boundary Layer Cloud Observations in the Azores, J. Climate, 25, 7381–7398, https://doi.org/10.1175/JCLI-D-11-00610.1, 2012.

Sandu, I., Brenguier, J., Geoffroy, O., Thouron, O., and Masson, V.: Aerosol impacts on the diurnal cycle of marine stratocumulus, J. Atmos. Sci., 65, 2705–2718, 2008.

Sandu, I., Brenguier, J.-L., Thouron, O., and Stevens, B.: How important is the vertical structure for the representation of aerosol impacts on the diurnal cycle of marine stratocumulus? Atmos. Chem. Phys., 9, 4039–4052, doi:10.5194/acp-9-4039-2009, 2009.

Sato, Y., Goto, D., Michibata, T., Suzuki, K., Takemura, T., Tomita, H., and Nakajima, T.: Aerosol effects on cloud water amounts were successfully simulated by a global cloud-system resolving model, Nat. Commun., 9, 985, https://doi.org/10.1038/s41467-018-03379-6, 2018.

https://doi.org/10.5194/egusphere-2023-1676
Preprint. Discussion started: 23 August 2023

Small, J., Chuang, P., Feingold, G. & Jiang, H.: Can aerosol decrease cloud lifetime? Geophys. Res. Lett. 36, L16806, 2009.

Stevens, B. and Feingold, G.: Untangling aerosol effects on clouds and precipitation in a buffered system, Nature, 461, 607–613, doi:10.1038/nature08281, 2009.

Stevens, B. & Seifert, A.: Understanding the macrophysical outcomes of microphysical choices in simulations of shallow cumulus convection. J. Meteorol. Soc. Jpn 86A, 141–163, 2008.

Sun-Mack, S., Minnis, P., Chen, Y., Kato, S., Yi, Y., Gibson, S. C., et al.: Regional apparent boundary layer lapse rates determined from CALIPSO and MODIS data for cloud-height determination. Journal of Applied Meteorology and Climatology, 53(4), 990–1011, 2014.

Terai, C. R., Wood, R., Leon, D. C., and Zuidema, P.: Does precipitation susceptibility vary with increasing cloud thickness in marine stratocumulus? Atmos. Chem. Phys., 12, 4567–4583, doi:10.5194/acp-12-4567-2012, 2012.

Terai, C. R., Wood, R., and Kubar, T. L.: Satellite estimates of precipitation susceptibility in low-level marine stratiform clouds, J. Geophys. Res., 120, 8878–8889, doi:10.1002/2015JD023319, 2015.

Toll, V., Christensen, M., Quaas, J., and Bellouin, N.: Weak average liquid-cloud-water response to anthropogenic aerosols, Nature, 572, 51–55, https://doi.org/10.1038/s41586-019-1423-9, 2019.

Trepte, Q. Z., and Coauthors: Global cloud detection for CERES edition 4 using Terra and Aqua MODIS data. IEEE Trans. Geosci. Remote Sens., 57, 9410–9449, https://doi.org/10.1109/TGRS.2019.2926620, 2019.

Twomey, S.: The Influence of Pollution on the Shortwave Albedo of Clouds, J. Atmos. Sci., 34, 1149–1152, https://doi.org/10.1175/1520-0469(1977)034<1149:TIOPOT>2.0.CO;2, 1977.

Wang, S., Wang, Q., and Feingold, G.: Turbulence, Condensation, and Liquid Water Transport in Numerically Simulated Nonprecipitating Stratocumulus Clouds, J. Atmos. Sci., 60, 262–278, https://doi.org/10.1175/1520-0469(2003)060<0262:TCALWT>2.0.CO;2, 2003.

Warren, S. G., C. J. Hahn, J. London, R. M. Chervine, and R. L. Jenne: Global distribution of total cloud cover and cloud type amounts over ocean, Tech. Note NCAR/TN-317 + STR, 42, Natl. Cent. for Atmos. Res., Boulder, Colo., https://doi.org/10.2172/5415329, 1988.

Williams, A. S., & Igel, A. L.: Cloud top radiative cooling rate drives non-precipitating stratiform cloud responses to aerosol concentration. Geophysical Research Letters, 48, e2021GL094740. https://doi.org/10.1029/2021GL094740, 2021.

Wood, R.: Stratocumulus Clouds, Mon. Weather Rev., 140, 2373–2423, https://doi.org/10.1175/MWR-D-11-00121.1, 2012.

Wu, P., Dong, X., Xi, B., Tian, J., & Ward, D. M.: Profiles of MBL cloud and drizzle microphysical properties retrieved from ground-based observations and validated by aircraft in situ measurements over the Azores. Journal of Geophysical Research: Atmospheres, 125, e2019JD032205. https://doi.org/10.1029/2019JD032205, 2020.

Wu, P., X. Dong, and B. Xi: A climatology of marine boundary layer cloud and drizzle properties derived from ground-based observations over the Azores. J. Climate, 33, 10133–10148, https://doi.org/10.1175/JCLI-D-20-0272.1, 2020.

Xi, B., Dong, X., Minnis, P., & Khaiyer, M. M.: A 10 year climatology of cloud fraction and vertical distribution derived from both surface and GOES observations over the DOE ARM SPG site. *Journal of Geophysical Research*, *115*(D12). https://doi.org/10.1029/2009jd012800, 2010

Xue, H. and Feingold, G.: Large-Eddy Simulations of Trade Wind Cumuli: Investigation of Aerosol Indirect Effects, J. Atmos. Sci., 63, 1605–1622, https://doi.org/10.1175/JAS3706.1, 2006.

Yeom, J. M., Yum, S. S., Shaw, R. A., La, I., Wang, J., Lu, C., et al.: Vertical variations of cloud microphysical relationships in marine stratocumulus clouds observed during the ACE ENA campaign. Journal of Geophysical Research: Atmospheres, 126, e2021JD034700. https://doi.org/10.1029/2021JD034700, 2021.

Zhang, Z., Song, Q., Mechem, D. B., Larson, V. E., Wang, J., Liu, Y., Witte, M. K., Dong, X., and Wu, P.: Vertical dependence of horizontal variation of cloud microphysics: observations from the ACE-ENA field campaign and implications for warm-rain simulation in climate models, Atmos. Chem. Phys., 21, 3103–3121, https://doi.org/10.5194/acp-21-3103-2021, 2021.

Zhang, J., Zhou, X., Goren, T., and Feingold, G.: Albedo susceptibility of northeastern Pacific stratocumulus: the role of covarying meteorological conditions, Atmos. Chem. Phys., 22, 861–880, https://doi.org/10.5194/acp-22-861-2022, 2022.

Zhang, J., and Feingold, G.: Distinct regional meteorological influences on low-cloud albedo susceptibility over global marine stratocumulus regions, Atmos. Chem. Phys., 23, 1073–1090, https://doi.org/10.5194/acp-23-1073-2023, 2023.

Zheng, Q., and Miller, M. A.: Summertime Marine Boundary Layer Cloud, Thermodynamic, and Drizzle Morphology over the Eastern North Atlantic: A Four-Year Study, J. Climate, 35, 4805-4825, https://doi.org/10.1175/JCLI-D-21-0568.1, 2022

Zhou, X., Zhang, J., & Feingold, G.: On the importance of sea surface temperature for aerosol-induced brightening of marine clouds and implications for cloud feedback in a future warmer climate. Geophysical Research Letters, 48, e2021GL095896. https://doi org/10.1029/2021GL095896, 2021

Zuidema, P., Leon, D., Pazmany, A., & Cadeddu, M.: Aircraft millimeter-wave passive sensing of cloud liquid water and water vapor during VOCALS-REx. *Atmospheric Chemistry and Physics*, *12*(1), 355-369. https://doi.org/10.5194/acp-12-355-2012, 2012